Neurobiology of Stress 25 (2023) 100546

Contents lists available at ScienceDirect

Neurobiology of Stress

journal homepage: www.elsevier.com/locate/ynstr

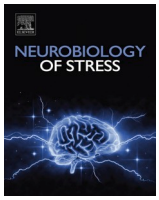

Post-weaning social isolation in male mice leads to abnormal aggression and disrupted network organization in the prefrontal cortex: Contribution of parvalbumin interneurons with or without perineuronal nets

Laszlo Biro [a,1,2,**], Christina Miskolczi [a,b,1], Huba Szebik [a,b], Biborka Bruzsik [a], Zoltan Kristof Varga [a], Laszlo Szente [a,b], Mate Toth [a], Jozsef Halasz [a,3], Eva Mikics [a,*]

[a] Institute of Experimental Medicine, Laboratory of Translational Behavioural Neuroscience, 1083 Budapest, Szigony utca 43., Hungary
[b] Janos Szentagothai Doctoral School of Neurosciences, Semmelweis University, 1085 Budapest, Ulloi ut 26., Hungary

ARTICLE INFO

Handling Editor: Dr. Tallie Z Baram

Keywords:
Aggression
Social
Isolation
Prefrontal
Parvalbumin
Perineuronal

ABSTRACT

Adverse social experiences during childhood increase the risk of developing aggression-related psychopathologies. The prefrontal cortex (PFC) is a key regulator of social behavior, where experience-dependent network development is tied to the maturation of parvalbumin-positive (PV+) interneurons. Maltreatment in childhood could impact PFC development and lead to disturbances in social behavior during later life. However, our knowledge regarding the impact of early-life social stress on PFC operation and PV+ cell function is still scarce. Here, we used post-weaning social isolation (PWSI) to model early-life social neglect in mice and to study the associated neuronal changes in the PFC, additionally distinguishing between the two main subpopulations of PV+ interneurons, i.e. those without or those enwrapped by perineuronal nets (PNN). For the first time to such detailed extent in mice, we show that PWSI induced disturbances in social behavior, including abnormal aggression, excessive vigilance and fragmented behavioral organization. PWSI mice showed altered resting-state and fighting-induced co-activation patterns between orbitofrontal and medial PFC (mPFC) subregions, with a particularly highly elevated activity in the mPFC. Surprisingly, aggressive interaction was associated with a higher recruitment of mPFC PV+ neurons that were surrounded by PNN in PWSI mice that seemed to mediate the emergence of social deficits. PWSI did not affect the number of PV+ neurons and PNN density, but enhanced PV and PNN intensity as well as cortical and subcortical glutamatergic drive onto mPFC PV+ neurons. Our results suggest that the increased excitatory input of PV+ cells could emerge as a compensatory mechanism for the PV+ neuron-mediated impaired inhibition of mPFC layer 5 pyramidal neurons, since we found lower numbers of GABAergic PV+ puncta on the perisomatic region of these cells. In conclusion, PWSI leads to altered PV-PNN activity and impaired excitatory/inhibitory balance in the mPFC, which possibly contributes to social behavioral disruptions seen in PWSI mice. Our data advances our understanding on how early-life social stress can impact the maturing PFC and lead to the development of social abnormalities in adulthood.

1. Introduction

Aggression-related psychopathologies have consistently been associated with a history of maltreatment in early life (Carr et al., 2013). Neglect is the most prevalent subtype of child maltreatment, with negative consequences comparable to, if not more detrimental than those of sexual or physical abuse (Gilbert et al., 2009; Stoltenborgh et al., 2015). Childhood and the adolescent period represent critical time

* Corresponding author.
** Corresponding author.
E-mail addresses: biro.laszlo@koki.hu (L. Biro), miskolczi.christina@koki.hu (C. Miskolczi), szebik.huba@koki.hu (H. Szebik), bruzsikbiborka@gmail.com (B. Bruzsik), varga.zoltan@koki.hu (Z.K. Varga), szente.laszlo@koki.hu (L. Szente), toth.mate@koki.hu (M. Toth), halasz.jozsef@amk.uni-obuda.hu (J. Halasz), mikics.eva@koki.hu (E. Mikics).
[1] Equal contribution.
[2] LB's current affiliation is Institute of Experimental Medicine, Laboratory of Thalamus Research, 1083 Budapest, Szigony utca 43., Hungary.
[3] JH's current affiliation is Obuda University, 8000 Szekesfehervar, Budai ut 45., Hungary.

https://doi.org/10.1016/j.ynstr.2023.100546
Received 3 April 2023; Received in revised form 10 May 2023; Accepted 28 May 2023
Available online 29 May 2023

windows during which brain regions modulating social behavior undergo major network reorganization (Blakemore, 2008). The prefrontal cortex (PFC) plays an integral role in the organization and execution of social behavior, including aggression (Lotze et al., 2007; Yang and Raine, 2009; Biro et al., 2018; Takahashi, 2022). The development of the PFC peaks in adolescence (Petanjek et al., 2011; Juraska and Willing, 2017; Kolk and Rakic, 2022), making it especially vulnerable to early-life stress (van Harmelen et al., 2010; Kelly et al., 2013). Adverse social experience could therefore disrupt maturation and lead to the emergence of abnormal social behavior, but the exact mechanisms behind this transition remain unknown.

Similarly to human studies, our prior research modelling child neglect shows that post-weaning social isolation (PWSI) in male rats leads to abnormal aggression in adulthood that disregards species-specific rules (e.g. PWSI rats deliver more attacks and a larger portion of the attacks are aimed at vulnerable body parts of the opponent) and disturbances in social behavior, including behavioral fragmentation (i.e. rapid abnormal switching between social behavioral elements) and increased defensive behavior (Tóth et al., 2008; Toth et al., 2011, 2012; Biro et al., 2017). Although behavioral studies in mice are rapidly gaining importance because of the increasing use of transgenic techniques, detailed characterization of PWSI-induced behavioral alterations has not been performed yet.

In PWSI rats, disturbances in social behavior are accompanied by structural changes in the PFC, including reduced thickness of the medial PFC (mPFC), a decrease in dendritic and glial density, and reduced vascularization (Biro et al., 2017). Additionally to structural deficits, PWSI leads to hyperactivity of selective PFC regions following aggressive interaction, including the infralimbic (IL), prelimbic (PrL) and anterior cingulate cortex (ACC) (Toth et al., 2012; Biro et al., 2017). These results suggest that PWSI-induced social disturbances involve the simultaneous contribution of various prefrontal subregions (Biro et al., 2018), but information on the dynamic interaction between them is very limited. The use of state-of-the-art methods for in vivo recording and manipulation of neural activity, while offering the benefit of advanced spatiotemporal resolution, have resulted in a tendency to selectively focus on single regions of the PFC without considering the importance of balanced interactions across multiple subregions in social behavior. Therefore, studies involving the large-scale investigation of various subregions and the interplay between these provide an important basis from where promising targets can be singled out.

Parvalbumin-expressing (PV+) interneurons, the most abundant interneuron subtype of the neocortex, form the backbone of prefrontal network activity (Sohal et al., 2009; Courtin et al., 2014; Kim et al., 2016). By exerting precise temporal control over surrounding pyramidal neurons, PV+ neurons maintain the excitatory/inhibitory (E/I) balance, increasing the efficiency of cortical information processing (Tremblay et al., 2016).

Experience-dependent development in the neocortex is tied to the maturation of parvalbumin-expressing interneurons (PV+ INs) and the appearance of perineuronal nets (PNNs) (Hensch, 2004; Larsen and Luna, 2018). PV+ basket cells can form two main subpopulations based on whether they are surrounded by perineuronal nets (PV+PNN+) or lack PNN (PV+PNN-) (Carulli and Verhaagen, 2021). PNNs are specialized extracellular matrix components that enwrap the perisomatic region of a great portion of PV+ neurons and are involved in the stabilization of synapses, restricting plasticity and promoting the closure of experience-dependent development (Carulli and Verhaagen, 2021).

Previous studies have shown that PFC PV+ neurons are involved in social behavior (Bicks et al., 2020), including aggression (van Heukelum et al., 2019; Li et al., 2022). Early-life stress has been shown to impact PV+ interneuron maturation and PNN development (Ueno et al., 2017a; Santiago et al., 2018; Murthy et al., 2019), and also cause disturbances in PV+ activity during social behavior (Bicks et al., 2020). Still, although numerous evidence points to a close relationship between PV+ interneuron maturation and PNN appearance in critical period plasticity and social experience-dependent learning, there is a staggering lack of knowledge on the specific role and properties of the prefrontal PV+PNN+ interneuron subpopulation itself. An added difficulty is that current in vivo targeting or recording methods do not allow for the reliable differentiation between prefrontal PV+PNN+ and PV+PNN- interneurons. Therefore, the role of each subpopulation in the regulation of social behavior, whether early-life stress impacts the two subpopulations in a distinct way, and whether these potential changes contribute to PWSI-induced abnormal social behavior remain to be elucidated.

Prefrontal PV+ interneurons and PNNs mature over the adolescent period (Ueno et al., 2017b), during which synaptic inputs arriving onto PV+ interneurons are also remodeled (Wang and Gao, 2010). Out of all interneurons, PV+ INs receive the strongest excitatory drive (Gulyás et al., 1999), which also renders them vulnerable to stressors (Ruden et al., 2021). Disturbances in glutamatergic drive of PV+ INs and the associated abnormal gamma oscillations have been implicated in various neuropsychiatric disorders, including schizophrenia (Ruden et al., 2021). These suggest that early-life isolation could impact PV+ interneuron function via altered input properties of PV+ interneurons. But whether these changes exist and are limited to a specific population of PV+ INs has not been examined as of yet. PNNs regulate the structure and connectivity of PV+ neurons, as it has been shown that PV+PNN+ interneurons display an increased density of perisomatic excitatory and inhibitory puncta, higher PV expression and longer axon initial segment compared to PV+PNN- interneurons (Carceller et al., 2020). Given the role of PNNs in PV+ IN development and protection against environmental stressors (Cabungcal et al., 2013), early-life adversities that perturb PNN maturation could ultimately impact the function of the PV+PNN+ population, whereas lack of PNN in the PV+PNN- INs could prove to be an added vulnerability in the face of adversity.

Here we aimed to characterize lasting behavioral changes following early-life social isolation in mice and to investigate the relationship between isolation-induced social deficits and the prefrontal PV+ interneuron- and PNN-network across multiple PFC subregions. We hypothesized that PWSI induces disturbances in the maturation of PV+ neurons and surrounding PNNs, potentially affecting the input and output properties of these neurons. We also hypothesized that PWSI differentially impacts the function of PV+PNN- and PV+PNN+ interneurons, which may play distinct roles in the regulation of social behavior. Impaired inhibition could then lead to altered intracortical dynamics and cause disruptions in prefrontal information processing, resulting in the expression of social deficits, including abnormal aggression, in adulthood.

2. Methods

2.1. Animals

All experimental subjects were male Crl:CD1 mice (Charles-River Laboratories) obtained from the breeding facility of the Institute of Experimental Medicine (Budapest, Hungary). Mice were maintained at a temperature of 22 ± 1 °C and at a relative humidity of 60 ± 10%, in a light-dark cycle of 12:12 h with lights off at 7AM and on at 7PM. Food and water were available ad libitum, except for the delay discounting training and test. Body weights of mice were regularly measured and did not differ between groups at any time point. Following weaning on postnatal day 21 (PN21), mice were randomly assigned to social (4 mice per cage) or isolation rearing (individually housed) in Plexiglas cages measuring 36,5 × 20,7 × 14 cm. Intruders used in the resident-intruder test were also male Crl:CD1 mice of the same source and were housed socially (4–5 mice per cage), under similar conditions. All experiments were carried out in accordance with the Directive of the European Parliament and the Council from 22 September 2010 (2010/63/EU) and were reviewed and approved by the Animals Welfare Committee of the Institute of Experimental Medicine.

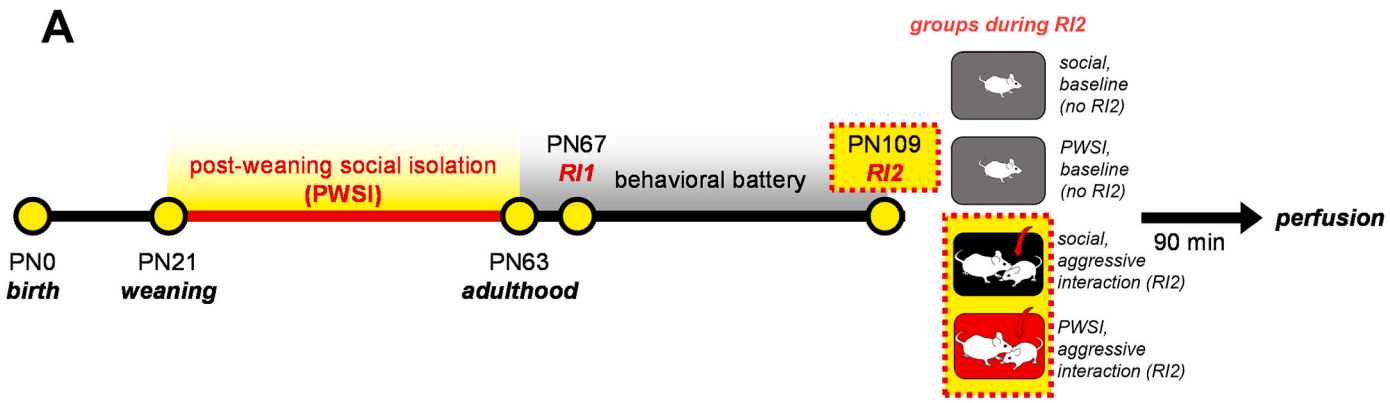

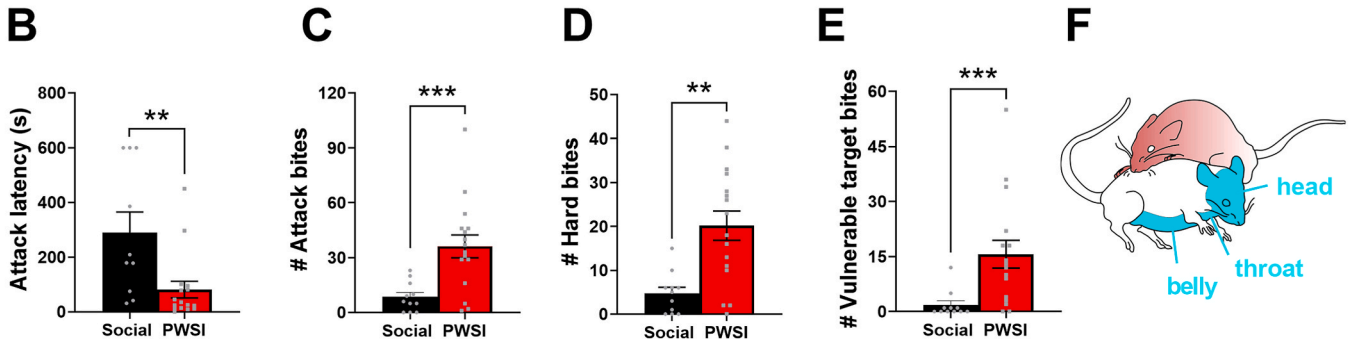

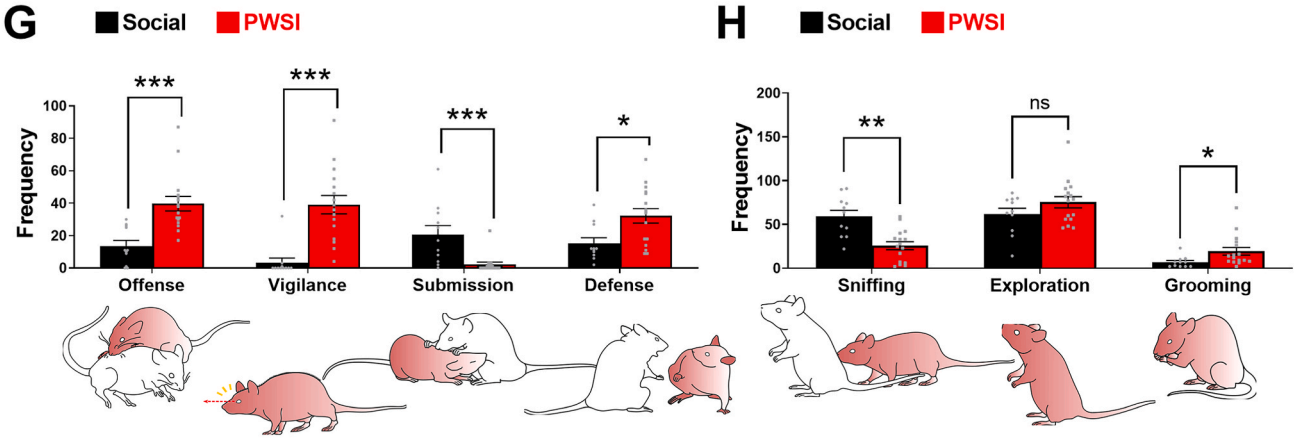

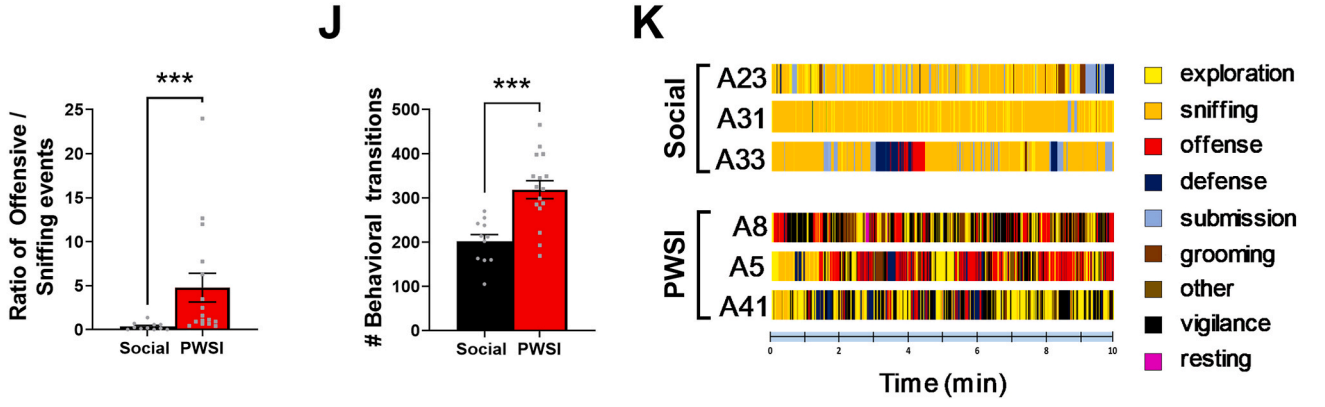

(caption on next page)

Fig. 1. Post-weaning social isolation (PWSI) induced abnormal aggression in conjunction with behavioral fragmentation. *A*, Experimental timeline. Following weaning, mice were housed individually (PWSI) for 6 weeks or were housed in groups of four (social). After reaching adulthood (PN63), mice were subjected to a behavioral battery. Data shown in *B–K* is from the second resident-intruder (RI) test at PN109, highlighted in red-bordered yellow. *B-D*, PWSI mice displayed shorter attack latencies, increased number of attack bites and hard bites compared to social mice in the RI test. *E-F*, Schematic drawing depicting the vulnerable body parts (head, throat, belly) which were targeted preferentially by PWSI mice. *G*, Frequency of agonistic behaviors recorded during the RI test. PWSI mice showed increased offense, vigilance, defense and reduced submission frequency. *H*, Frequency of non-agonistic behaviors recorded during the RI test. PWSI mice showed reduced sniffing and increased grooming frequency. *I*, PWSI mice had an increased ratio of offensive/sniffing events in the RI test. *J*, PWSI mice showed behavioral fragmentation as indexed by the number of behavioral transitions in the RI test. *K*, Representative temporal raster plots comparing the behavioral organization of three social (top panels) and three PWSI (bottom panels) mice during the RI test. All data are represented as mean ± SEM. *p < 0.05, **p < 0.01, ***p < 0.001. A, animal; PN, postnatal day; RI, resident-intruder test. (For interpretation of the references to color in this figure legend, the reader is referred to the Web version of this article.)

2.2. Experimental design

Upon weaning, mice were housed individually (post-weaning social isolation; PWSI) for 6 weeks or were housed in groups of four (social rearing). In order to eliminate litter effects, mice from all litters were randomly assigned to PWSI or social rearing. The members of socially-reared groups came from different litters. After reaching adulthood (PN63), mice were subjected to a behavioral test battery that lasted from PN64 to PN109 (see Figs. 1A and 2A for timeline and Supplementary Fig. S1A for detailed timeline; note that all three refer to the same experiment). Behavioral experiments were performed during the first half of the dark (active) cycle, beginning at 8–9AM. On PN64, following the open field test, all experimental mice were subjected to single housing and remained so for subsequent tests. A resident-intruder (RI) test was conducted on PN67 (RI1) to verify the appearance of the PWSI-induced aggressive phenotype described in our previous studies in rats (Tóth et al., 2008; Toth et al., 2011), and a second RI test (RI2) was conducted following the behavioral battery, on PN109, to ensure that the aggressive phenotype remained stable over time and to investigate aggressive interaction-induced changes in the prefrontal cortex (see Fig. 1A for timeline).

On PN109, mice were perfused under resting conditions or 90 min after the second resident-intruder test. Sample size for PWSI mice was N = 22, and for social mice N = 20. All animals underwent the behavioral test battery, with the exception of the RI2 test on PN109, where animals were split into 4 groups: "social, baseline" (i.e. did not undergo RI2, N = 6), "PWSI, baseline" (did not undergo RI2, N = 6), "social, aggressive interaction" (underwent RI2, N = 14) and "PWSI, aggressive interaction" (underwent RI2, N = 16). In this way, every animal was subjected to the same effects up until the split, while the split itself was made to ensure that baseline control groups were available for our histological analyses (i.e. resting conditions versus fighting-induced prefrontal activation). Sample size varied slightly between tests due to minor technical issues (e.g. damaged video record). 2 social mice were excluded from the final analysis because of statistically extremely outlying behavioral parameters in the resident-intruder tests (i.e. total bite and vulnerable target bite values were over 3 standard deviations above the mean, for further description of biting attacks refer to 2.3.2).

2.3. Behavioral test battery

2.3.1. Open field test (OF)

The OF was a square black Plexiglas box measuring 40 × 36 × 15 cm. Subjects were placed into the middle of the box and were allowed to roam the apparatus for 10 min under low light illumination (70 lux). The apparatus was cleaned with water and dried thoroughly between tests. Behavior was video-recorded and subsequent manual analysis was performed by a blind experimenter using the H77+ event-recording software (Jozsef Haller, Institute of Experimental Medicine, Budapest, Hungary). Locomotion was measured by the number of line-crossings using a grid placed over the recording. Other parameters investigated were latency to enter the center and percentage of time spent in the center. The center area was defined as the central 20 × 18 cm zone of the apparatus.

2.3.2. Resident-intruder tests (RI) and escalation

3 days prior to the first RI test, all experimental (i.e. resident) mice were transferred into individual cages with fresh corn cob bedding. This was done to allow for the emergence of territorial behavior. **Resident-intruder tests:** in the early hours of the dark cycle (i.e. 8-9AM) under dim red illumination, a novel, smaller-sized male intruder was placed into the homecage of the resident for 10 min. Behavior was recorded and analyzed as described below. **Escalation:** in the early hours of the dark cycle (i.e. 8-9AM) under dim red illumination, a smaller-sized male opponent was placed into the subject's homecage for 5 min in a wire box measuring 18 × 12 × 10 cm. The resident could see and smell the opponent but could not make direct contact with it (de Almeida, 2002). Following the escalation period, the wire box and opponent were removed and a novel smaller-sized male intruder was placed into the homecage of the resident for 10 min. Behavior was recorded and analyzed as described below. On PN109, mice were either perfused under resting conditions or 90 min after the second RI test. Behavior was recorded and analyzed at low speed, with frame-by-frame analysis when necessary, by an experimenter blinded to the conditions. We investigated the latency to first biting attack, the number of biting attacks, their intensity (soft versus hard bites) and whether the attacks were aimed at vulnerable body parts of the opponent, i.e. the head, throat or belly (see Fig. 1F) (Tóth et al., 2008; Toth et al., 2011). Hard bites were defined as biting attacks given with a forceful body movement of the resident, inducing a strong startle response in the intruder (large jump or defensive behavior). Soft bites were not accompanied by excessive movement and induced a mild response from the intruder at most (Tóth et al., 2008). Additionally, we analyzed the duration and frequency of each behavioral type using the Solomon Coder event-recording software (RRID:SCR_016041). Main categories were as follows: exploration (rearing and exploratory activity that is not directed towards the conspecific), sniffing (non-aggressive sniffing of any body part of the opponent), grooming (self-grooming movements), offensive behavior (chasing, attack bouts, tail-rattling, aggressive grooming, mounting, punching and kicking), defensive behavior (fleeing from the opponent, defensive upright posture), submission (being unmoving while being sniffed or aggressively groomed by the conspecific, usually crouched low with closed eyes) and vigilance (continuous tense or agitated observation of the intruder from a distance, with the body constantly being directed toward the intruder) (Duque-Wilckens et al., 2018; Newman et al., 2019).

2.3.3. Social interaction test (SI)

Two unfamiliar experimental mice of the same housing group (i.e. isolated versus isolated, social versus social) were placed into a novel Plexiglas test cage measuring 35 × 20 × 25 cm under low light illumination (70 lux). Each animal was separately habituated to the novel cage the day before testing for 15 min. On PN72, the pairs were placed into the cage for 10 min and their behavior was video-recorded and analyzed. Behavioral parameters investigated were the duration and frequency of exploration, sniffing, defensive behaviors, aggressive behaviors, grooming and digging activities.

2.3.4. Delay discounting test

The protocol used here was based on the work of Adriani et al. (2003)

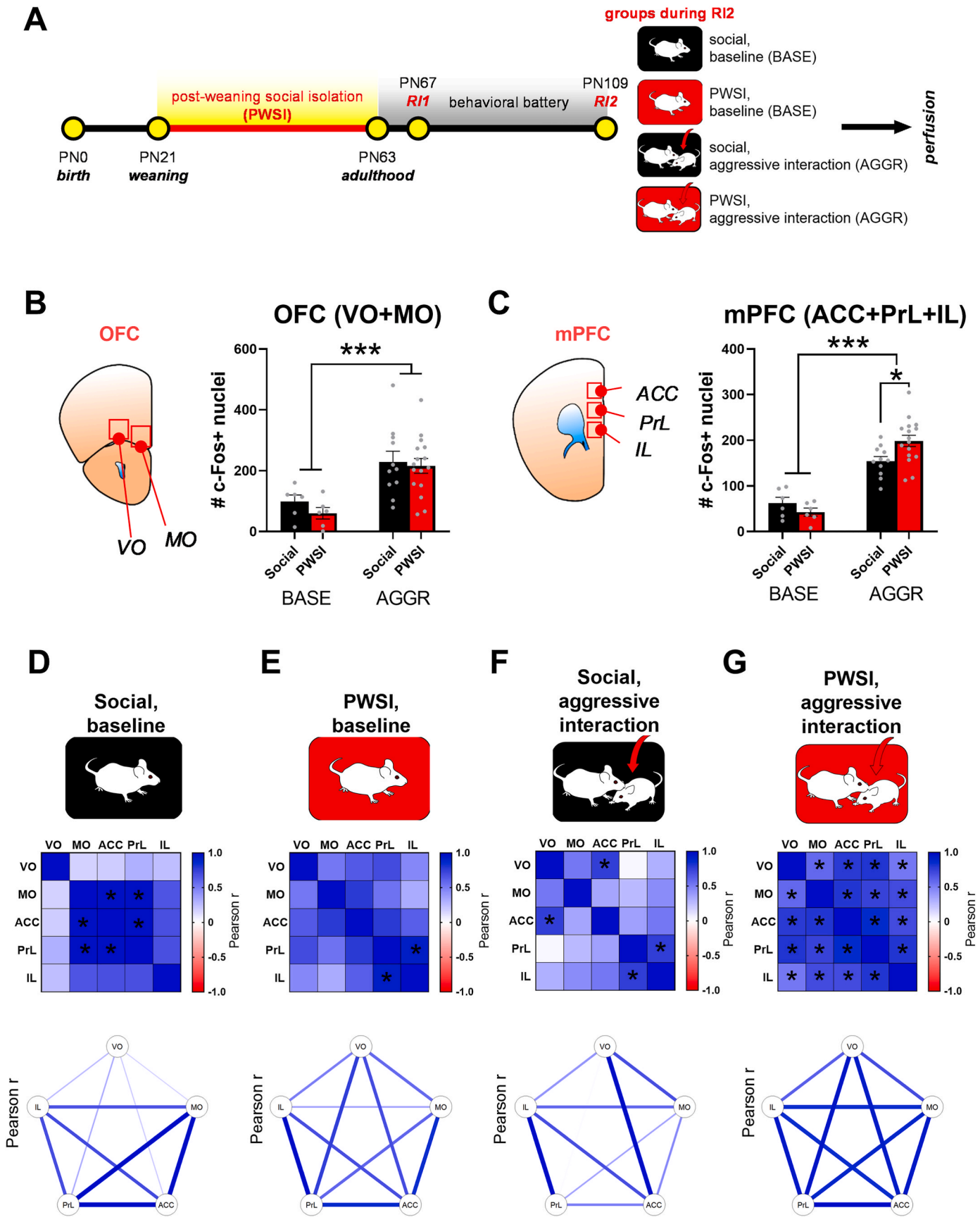

(caption on next page)

Fig. 2. PWSI-induced abnormal aggression is associated with subregion-specific neuronal hyperactivation in the mPFC and disrupted co-activation patterns across mPFC and OFC subregions. *A*, Experimental design. Upon weaning, mice were housed individually (PWSI) or were housed in groups of four (social). After reaching adulthood mice were subjected to a behavioral test battery. On PN109, mice were perfused under baseline conditions (BASE) or 90 min after the aggressive interaction (AGGR) followed by c-Fos immunostaining to investigate the impact of PWSI on the neuronal activation of the PFC. *B–C, Aggressive interaction induced an mPFC-specific enhanced c-Fos expression in PWSI mice compared to social mice. B*, Schematic drawing showing the Bregma level of the investigated orbitofrontal (OFC) subregions and bar graph showing the number of c-Fos immuno-positive nuclei within the OFC, including the ventral orbitofrontal (VO) and medial orbitofrontal cortices (MO). *C*, Schematic drawing showing the Bregma level of the investigated medial prefrontal (mPFC) subregions and bar graph showing the number of c-Fos immuno-positive nuclei within the mPFC, including the anterior cingulate (ACC), the prelimbic (PrL) and the infralimbic cortices (IL). *D-G, PWSI induced disrupted functional connectivity across PFC subregions.* Cross-correlation and network connectivity analysis of c-Fos expression in experimental groups, computed as covariance across subjects to reveal interactions between PFC subregions. The top row represents the complete set of interregional correlations in each experimental group, whereas the bottom row depicts node graphs where the nodes represent brain regions and the width of connections between nodes indicate the higher correlation coefficients. Connectivity matrices and node graphs representing social BASE (*D*), PWSI BASE (*E*), social AGGR (*F*) and PWSI AGGR (*G*) groups. Colors indicate Pearson correlation coefficients (scale, right) and labels within squares correspond to p values of correlations. All data are represented as mean ± SEM. *p < 0.05, **p < 0.01, ***p < 0.001. ACC, anterior cingulate cortex; AGGR, aggressive interaction; BASE, baseline condition; IL, infralimbic cortex; MO, medial orbitofrontal cortex, mPFC, medial prefrontal cortex; OFC, orbitofrontal cortex; PN, postnatal day; PrL, prelimbic cortex, RI1, first resident-intruder test; RI2, second resident-intruder test; VO, ventral orbitofrontal cortex. (For interpretation of the references to color in this figure legend, the reader is referred to the Web version of this article.)

and Aliczki et al. (2014). The test took place in automated operant chambers equipped with two nose-poke holes with LED lights and infrared sensors, a feeding device with a magazine where sugar pellets were held, and a chamber light (Med Associates, St. Albans, VT, USA). The chambers were each placed into sound-attenuated wooden cubicles and were controlled via the Med-PC IV software (Med Associates, St. Albans, VT, USA). The chambers were cleaned with 20% ethanol and were dried before each trial. Four days before the start of the experiment, mice were subjected to a restricted feeding protocol (maintaining 85–95% of their original body weight) to increase their motivation for food rewards. **Training phase:** mice were placed into the chambers daily for 30 min during 8 consecutive days. Nose-poke responses given into one of the holes were rewarded with one 45 mg sugar pellet (small reward), whereas responses given into the other hole were rewarded with three 45 mg pellets (large reward). Both types of rewards were each presented immediately after the response was given, and were followed by a 25 s timeout period during which responses were not rewarded but were registered. The side of the nose-poke hole (left or right) associated with the large reward was balanced over subjects. Over training, all mice developed a strong preference for the side that was associated with the large reward. **Test phase:** following training mice were subjected to a protocol similar to the training phase, but the delivery of the larger reward was preceded by a delay. Small rewards were still delivered immediately following the response. The delay of the large reward was progressively increased each day (5, 10, 20, 30, 45, 60, 75, 90 s from day 1 to day 8, respectively). Responses made during the delays and timeout periods were not rewarded but were recorded. Due to the increasing delay in delivery, mice gradually shifted their preference from the large reward to the immediate small reward. Motivational state of mice can be characterized by the number of total responses during training and testing, whereas inadequate responses (nose pokes for large reward during delay period and time out) are considered an indicator of impulsive responses (Dalley et al., 2008).

2.3.5. Elevated plus-maze (EPM)

The EPM was made of gray Plexiglas and consisted of two open arms (30 × 7 cm), two closed arms (30 × 7 cm with 30 cm high walls) and a central platform (7 × 7 cm) 50 cm above the ground. Subjects were placed into the central platform facing an open arm and were allowed to explore the apparatus for 5 min under low light illumination (70 lux). The EPM was cleaned with water and dried thoroughly between tests. Behavior was video-recorded and analyzed with the event-recording software Solomon Coder. Locomotion was measured via the number of closed arm entries. Other parameters included the percentage of time spent in the open arms and the ratio of open arm entries and total arm entries.

Table 1
Overview of primary antibodies or reagents used in this study.

Reagent	Source	Catalog No.	Host	Dilution	RRID
Bassoon	Abcam	SAP7F407	Mouse	1:1000	AB_1860018
c-Fos	Synaptic Systems	226 004	Guinea pig	1:4000 1:3000 IF	AB_2619946
Parvalbumin	Swant	PV27	Rabbit	1:5000 1:2500	AB_2631173
Parvalbumin	Sigma-Aldrich	P3088	Mouse	1:5000	AB_477329
Parvalbumin	Synaptic Systems	195 004	Guinea pig	1:2000	AB_2156476
vGAT	Synaptic Systems	131 004	Guinea pig	1:1000	AB_88787
vGluT1	Synaptic Systems	135 304	Guinea pig	1:1000	AB_887878
vGluT2	Synaptic Systems	135 402	Rabbit	1:1000	AB_2187539
Voltage-gated potassium channel type 2.1 (Kv2.1)	Neuromab	75–014	Mouse	1:1000	AB_10673392
Wisteria floribunda agglutinin (WFA)	Sigma-Aldrich	L1516	–	1:500	AB_2620171

2.3.6. Sucrose preference test (SPT)

A bottle filled with 2% sucrose solution was placed alongside the bottle containing drinking water in the homecage of the animals. The bottles were left there overnight and then measured on the next day for four consecutive days. The starting side of the sucrose solution bottle was balanced over subjects and the position of the sucrose solution bottle and water bottle was switched each day (i.e. left versus right). Sucrose preference was measured as the percentage of sucrose consumption (g) divided by total consumption (g).

2.4. Immunohistochemistry and imaging

2.4.1. Fixation and tissue processing

Mice were deeply anesthetized with a mixture of ketamine–xylazine (16.6 and 0.6 mg/ml, respectively). Subsequently, mice were transcardially perfused with ice-cold 0.1 M phosphate-buffered saline followed by 4% paraformaldehyde in 0.1 M phosphate-buffered saline solution (PBS), pH 7.4. Brains were dissected, removed and post-fixed for 3 h. They were then cryoprotected in 30% sucrose in PBS for 48 h at 4 °C. Following sucrose cryoprotection, 30 μm sections were cut on a freezing sliding microtome. Sections were collected in a six-well plate

Table 2
Overview of secondary antibodies used in this study.

Antibody	Source	Catalog No.	Host	Dilution	RRID
Alexa Fluor 488 anti-guinea pig IgG	Jackson ImmunoResearch	706-545-148	Donkey	1:200	AB_2340472
Alexa Fluor 488 anti-mouse IgG	Jackson ImmunoResearch	715-545-151	Donkey	1:500	AB_2341099
Alexa Fluor 488 anti-rabbit IgG	Jackson ImmunoResearch	711-545-152	Donkey	1:500	AB_2313584
Alexa Fluor 488 conjugated streptavidin	Jackson ImmunoResearch	016-540-084		1:500	AB_2337249
Alexa Fluor 647 anti-mouse IgG	Jackson ImmunoResearch	715-605-150	Donkey	1:500	AB_2340862
Alexa Fluor 647 anti-guinea pig IgG	Jackson ImmunoResearch	706-605-148	Donkey	1:500	AB_2340476
Alexa Fluor 647 anti-rabbit IgG	Jackson ImmunoResearch	711-605-152	Donkey	1:200	AB_2492288
Alexa Fluor 647 anti-rabbit IgG	Jackson ImmunoResearch	111-605-003	Goat	1:500	AB_2338072
Biotin conjugated anti-guinea pig IgG	Jackson ImmunoResearch	706-065-148	Donkey	1:1000	AB_2340451
Cy3-conjugated anti-guinea pig IgG	Jackson ImmunoResearch	106-165-003	Goat	1:500	AB_2337423
Cy3-conjugated anti-guinea pig IgG	Jackson ImmunoResearch	706-165-148	Donkey	1:500	AB_2340460
Cy3-conjugated anti-mouse IgG	Jackson ImmunoResearch	715-165-151	Donkey	1:200	AB_2315777
Cy3-conjugated anti-rabbit IgG	Jackson ImmunoResearch	711-165-152	Donkey	1:500	AB_2307443
DyL405 anti-mouse	Jackson ImmunoResearch	115-475-003	Goat	1:500	AB_2338786
DyL405 conjugated streptavidin	Jackson ImmunoResearch	016-470-084		1:500	AB_2337248

using cryoprotectant (50% sodium phosphate buffer, 30% ethylene glycol, 20% glycerol) as a storage solution and were kept at −20 °C.

2.4.2. c-Fos immunostaining for light microscopy

c-Fos immunohistochemistry was carried out on free-floating sections that were washed in PBS to remove the cryoprotectant as described earlier (Biro et al., 2017). After inactivation of endogenous peroxidases with 0.3% H_2O_2 containing 0.5% Triton X-100 and further PBS washings, the sections were incubated for 1 h in PBS containing 10% normal goat serum. Sections were then incubated in guinea-pig polyclonal anti-c-Fos antibody (see Table 1) in PBS with 3% NGS for 48 at 4 °C. The primary antibody was detected by biotinylated anti-guinea-pig donkey serum (1:1000 in PBS with 2.5% NGS; Jackson ImmunoResearch, see Table 2) and avidin–biotin complex (ABC, 1:1000; Vector Laboratories) for 1 h each at room temperature. The peroxidase reaction was developed in the presence of diaminobenzidine tetrahydrochloride (0.5 mg/ml), nickel–ammonium sulfate (0.1%) and hydrogen peroxide (0.003%) dissolved in Tris buffer for 5 min. Sections were mounted on Superfrost Plus microslides (VWR International, LLC) and dried on a drying rack overnight. Mounted sections were dehydrated in ascending ethanol solutions, cleared with xylene, and coverslipped with DPX (Sigma-Aldrich). Microscopic images were digitized by an Olympus CCD camera using a 20x magnification lens and c-Fos immunoreactive nuclei were counted using Fiji as described previously (Toth et al., 2012). To avoid any bias in the analysis, all slides were coded prior to analysis and remained so until the experiment was completed.

2.4.3. Fluorescent immunostaining, imaging and density analysis of the activated (c-Fos+) PV+PNN- and PV+PNN+ neurons

One series of sections were used for this immunostaining. After several PBS washes, sections were incubated in the following reagents: biotinylated *Wisteria floribunda* agglutinin (WFA), rabbit anti-parvalbumin antibody and guinea-pig anti-c-Fos antibody diluted in PBS containing 0.25% Triton-X100 and 1% bovine serum albumin (BSA) for 24 h at 20 °C (see Table 1). After being washed with PBS, the sections were incubated in a mixture of DyL405-conjugated donkey anti-goat IgG, Alexa 488-conjugated streptavidin, Cy3-conjugated goat anti-guinea pig IgG and Alexa647-conjugated donkey anti-rabbit IgG with 0.2% Triton-X100 for 2 h at 20 °C (see Table 2). After being washed with PBS, the sections were mounted on glass slides and coverslipped using Mowiol 4–88 fluorescent mounting medium and analyzed using Nikon C2 confocal microscope (Plan Apo VC 20x, NA = 0.75; xy, 1.24 μm/pixel; z-step size, 2 μm). Overview images (tiles) of orbitofrontal and prefrontal cortices were acquired by 405, 488, 561, and 642 nm lasers. Images were taken at levels 2.68−1.42 mm anterior from bregma. For the PV+/PNN+/c-Fos co-expression quantification, single-labeled, double-labeled and triple-labeled neurons were counted manually using NIS Elements Software (Nikon Europe; RRID:SCR_014329).

2.4.4. Fluorescent immunostaining, imaging and analysis of perisomatic puncta densities

The PFC-containing sections were incubated with a solution containing 2% Triton X-100 and 10% normal donkey serum (NDS) in 0.1 M PB for 4 h at room temperature. This was followed by a 4-day-long incubation at 4 °C in a solution containing 2% Triton X-100, 10% NDS, 0.05% sodium azide, and different combinations of the following primary antibodies and reagents: mouse anti-bassoon, rabbit anti-parvalbumin, mouse anti-parvalbumin, guinea pig anti-parvalbumin, guinea pig anti-vesicular GABA transporter (vGAT), guinea pig anti-vesicular glutamate transporter 1 (vGluT1), rabbit anti-vesicular glutamate transporter 2 (vGluT2), mouse anti-potassium voltage-gated channel, Shab-related subfamily, member 1 (Kv2.1) and biotinylated WFA (see Table 1).

The primary antibodies were visualized using the following secondary antibodies: DyL405-conjugated streptavidin, Alexa Fluor 488-conjugated donkey anti-guinea pig, Alexa Fluor 488-conjugated donkey anti-rabbit, Cy3-conjugated donkey anti-mouse IgG, Cy3-conjugated donkey anti-guinea pig IgG, Alexa647-conjugated donkey anti-rabbit IgG, Alexa647-conjugated donkey anti-mouse IgG (see Table 2).

Confocal images were collected at 12-bit depth and 1024 × 1024 pixel resolution using a Nikon A1R microscope fitted with an oil-immersion apochromatic lens (CFI Plan Apo VC60x Oil, NA 1.40; z step size: 0.5 μm; xy: 0.11 μm/pixel). We analyzed the density of puncta surrounding the soma of Kv2.1 immunoreactive putative pyramidal neurons and PV neurons using a similar methodology. In the mPFC, between 40 and 50 putative pyramidal neurons were imaged per animal in three different sections. From each animal, 10 to 15 PV neurons were counted per subregion, since their density was more limited. Images were processed using NIS Elements Software (Nikon Europe; RRID: SCR_014329). The profile of the cell membrane of every soma was delineated manually, and this selection was further enlarged by 0.25 μm in order to create a "ring" that covers the area surrounding the soma. For this analysis, we used the following criteria: vGluT1+Bassoon+ and vGluT2+Bassoon+ puncta in close proximity to PV+ or Kv2.1+ somata were considered to establish an apposition (i.e. form putative perisomatic synapses). Bassoon is a presynaptic release site marker (Dani et al., 2010), vGluT1 and vGluT2 denote excitatory intracortical and extracortical inputs, respectively (Takamori et al., 2000, 2001; Fremeau et al., 2001), whereas Kv2.1 immunoreactivity was used to identify pyramidal cells in layer 5 of the mPFC (Vereczki et al., 2016).

Labeling intensities of the perisomatic region and PV somata were quantified in arbitrary units as the mean of all selected pixels using custom scripts in Fiji. Intensities of single neurons were plotted. Previously drawn ROIs were used to measure mean fluorescent intensity and integrated density in the area ±0.25 μm from the cell border using custom scripts (Guirado et al., 2018).

2.5. Statistical analysis

Data are expressed as mean ± standard error of the mean (SEM). Differences between groups were analyzed using the Prism (GraphPad Prism Software Inc. San Diego, California, USA) or Statistica 13.5 (Tibco, Palo Alto, CA, USA) softwares by means of Student's t-test, or Mann-Whitney *U* test when requirements for t-tests were not fulfilled (i.e. when data did not follow a normal distribution, as investigated by the D'Agostino and Pearson normality test). In the case of the delay discounting experiment and sucrose preference test, we used repeated measures ANOVA. For c-Fos activation and PNN-dependent puncta analysis, we used two-way ANOVA, followed by Fisher's post hoc analyses. In the statistical analysis of individual cell numbers as a function of group, we implemented both the factor "housing" and "animal identity" in an additive fashion to a two-way ANOVA model. This way, we were able to determine the explanatory effects of the social environment and individual variability of animals independently (Supplementary Table 1). These latter analyses were performed in R Statistical Environment (R Core Team, 2022). The Pearson correlation coefficient or the Spearman rank correlation was applied to find the relationship between the values extracted from brain regions, behavioral variables and puncta densities or fluorescence intensities of PV+ neurons or PNNs. We controlled for the problem of multiple correlation analysis by using the false discovery rate (FDR) approach of Benjamini and Hochberg (1995). FDR compares the number of significant findings with the expected proportion of false positive findings, highlighting true positive discoveries this way. FDR is widely accepted for controlling multiplicity problems in high parameter data due to its superiority in power and equality in specificity to family-wise error rate-based approaches. The significance level was set at $p < 0.05$ throughout, all p values are indicated with exact numbers.

3. Results

3.1. Post-weaning social isolation (PWSI) induced abnormal aggression in conjunction with behavioral fragmentation and disrupted behavioral organization

We first aimed to characterize long-term behavioral consequences of PWSI on social and emotional function in mice by submitting them to a 6-week-long isolation period followed by a behavioral test battery (for detailed timeline, see Supplementary Fig. S1A).

PWSI led to enhanced aggression compared to socially-reared mice as seen in the second RI test (see Fig. 1A for timeline). Particularly, PWSI mice displayed shorter attack latencies ($U = 28$, $p = 0.005$; Fig. 1B) and delivered more bites ($U = 25.5$, $p = 0.001$; Fig. 1C). Detailed analysis of aggressive interactions revealed that PWSI mice targeted more bites toward vulnerable body parts of opponents, such as the head, throat and belly ($U = 24.5$, $p = 0.002$; Fig. 1E and F). Moreover, there was an increase in violent hard bites delivered by PWSI mice compared to social mice ($U = 27$, $p = 0.003$; Fig. 1D).

PWSI mice exhibited increased frequencies of offensive ($U = 12$, $p < 0.001$; Fig. 1G) and defensive ($U = 36.5$, $p = 0.010$; Fig. 1G) behavior and showed less submissive behavior ($U = 20$, $p < 0.001$; Fig. 1G) compared to the social group. Interestingly, we also observed that PWSI mice showed an increase in vigilance-like behavior (i.e. agitated observation of the intruder from a distance, with the body constantly being directed toward the intruder) (Duque-Wilckens et al., 2018; Newman et al., 2019) compared to social mice ($U = 6$, $p < 0.001$; Fig. 1G). PWSI mice spent less time with social investigation as indicated by a reduction in non-aggressive social sniffing ($U = 22$, $p = 0.001$; Fig. 1H). In turn, we also observed an increase in grooming behavior ($U = 35.5$, $p = 0.011$; Fig. 1H) compared to social mice. Importantly, the observed changes in offensive and sniffing behavior led to a considerable increase in the ratio of offense/sniffing events in PWSI mice ($U = 16$, $p < 0.001$; Fig. 1I). PWSI also caused a fragmented behavioral phenotype, indicated by the increased number of behavioral transitions (i.e. PWSI mice showed rapid shifting between behavioral elements) ($U = 16$, $p < 0.001$; Fig. 1J and K).

In order to verify the PWSI-induced aggressive phenotype previously reported in our rat studies (Tóth et al., 2008; Toth et al., 2011) and to ensure that PWSI-induced aggression remained stable following the behavioral battery, we conducted an RI test right after the early-life isolation period and another RI test following the behavioral battery, before perfusion. Changes in aggressive behavior were already present during the first RI conducted right after the early-life isolational period, on PN67 (see Fig. 1A for timeline) (significant differences between PWSI and social mice in total attack bites during first RI, $U = 95$, $p = 0.0152$; percentage of vulnerable target bites, $U = 70$, $p = 0.0008$; Supplementary Fig. S1B) and PWSI-induced abnormal aggression proved to be persistent over time, with the number of attack bites ($U = 25.5$, $p = 0.001$; Fig. 1C) and percentage of vulnerable target bites ($U = 33$, $p = 0.0048$; Supplementary Fig. S1C) remaining significantly elevated compared to social controls even after the behavioral battery.

Additionally, since emotionally driven reactive aggression is often characterized by excessive aggressive outbursts to a perceived provocation (Kempes et al., 2005), we hypothesized that PWSI could exacerbate social instigation-evoked escalated aggression (de Almeida, 2002) (Supplementary Fig. S1D). Consistent with our hypothesis, PWSI mice submitted to social instigation showed a robust increase in the frequency of attack bites ($U = 67.5$, $p < 0.001$; Supplementary Fig. S1E), hard bites ($U = 93.5$, $p = 0.007$; Supplementary Fig. S1F) and bites targeting vulnerable areas ($U = 54$, $p < 0.001$; Supplementary Fig. S1G).

3.2. PWSI induced social deficits and reduced motivation

Since PWSI heavily affected the social behavioral domain, indicated by an abnormal aggressive phenotype, we wondered whether reciprocal social interactions could also be affected in a less aggression-promoting context. Thus, to evaluate how PWSI affects the social behavioral repertoire in neutral territory (unfamiliar for subjects) when engaged with an unfamiliar, same-sized adult conspecific, we performed a social interaction test (SI, Supplementary Fig. S1H). We found that PWSI mice exhibited reduced sniffing frequency ($U = 91$, $p = 0.005$; Supplementary Fig. S1I), a trend to increased defensive behavior ($U = 127$, $p = 0.078$; Supplementary Fig. S1I), and we also observed an increase in the ratio of aggressive/social behavior compared to social mice ($U = 87$, $p = 0.003$; Supplementary Fig. S1J). Non-social parameters were not affected as PWSI mice showed a similar frequency of exploration ($U = 171$, $p = 0.833$; Supplementary Fig. S1I), grooming ($U = 162.5$, $p = 0.642$; Supplementary Fig. S1I), and digging ($U = 147.5$, $p = 0.354$; Supplementary Fig. S1I) compared to the social group.

Collectively, our data provide strong evidence that PWSI induces marked social deficits in conjunction with increased and abnormal forms of aggression.

Anxiety-like behavior was evaluated in the open-field test (OF, Supplementary Fig. S2A) and the elevated plus-maze (EPM, Supplementary Fig. S2E), respectively. PWSI did not affect anxiety-like behavior in the OF as both experimental groups showed similar locomotor activity ($U = 161.5$, $p = 0.477$; Supplementary Fig. S2B), time spent in the center ($U = 184$, $p = 0.901$; Supplementary Fig. S2C), and latency to enter the center ($U = 187$, $p = 0.967$; Supplementary Fig. S2D). Similarly, PWSI did not affect locomotion or anxiety parameters such as the frequency of closed arm entries ($U = 185.5$, $p = 0.927$; Supplementary Fig. S2F), the duration of open arm entries ($U = 173$, $p = 0.666$; Supplementary Fig. S2G), and the ratio of open arm entries/total entries ($U = 166.5$, $p = 0.535$; Supplementary Fig. S2H) in the EPM test, suggesting that the anxiety-like domain was not affected by PWSI.

Early-life adversities have been repeatedly linked to an altered motivational state and impulsivity in adulthood (Birnie et al., 2020; Sanchez and Bangasser, 2022). To explore such implications, PWSI mice were tested in the delay discounting paradigm using operant chambers

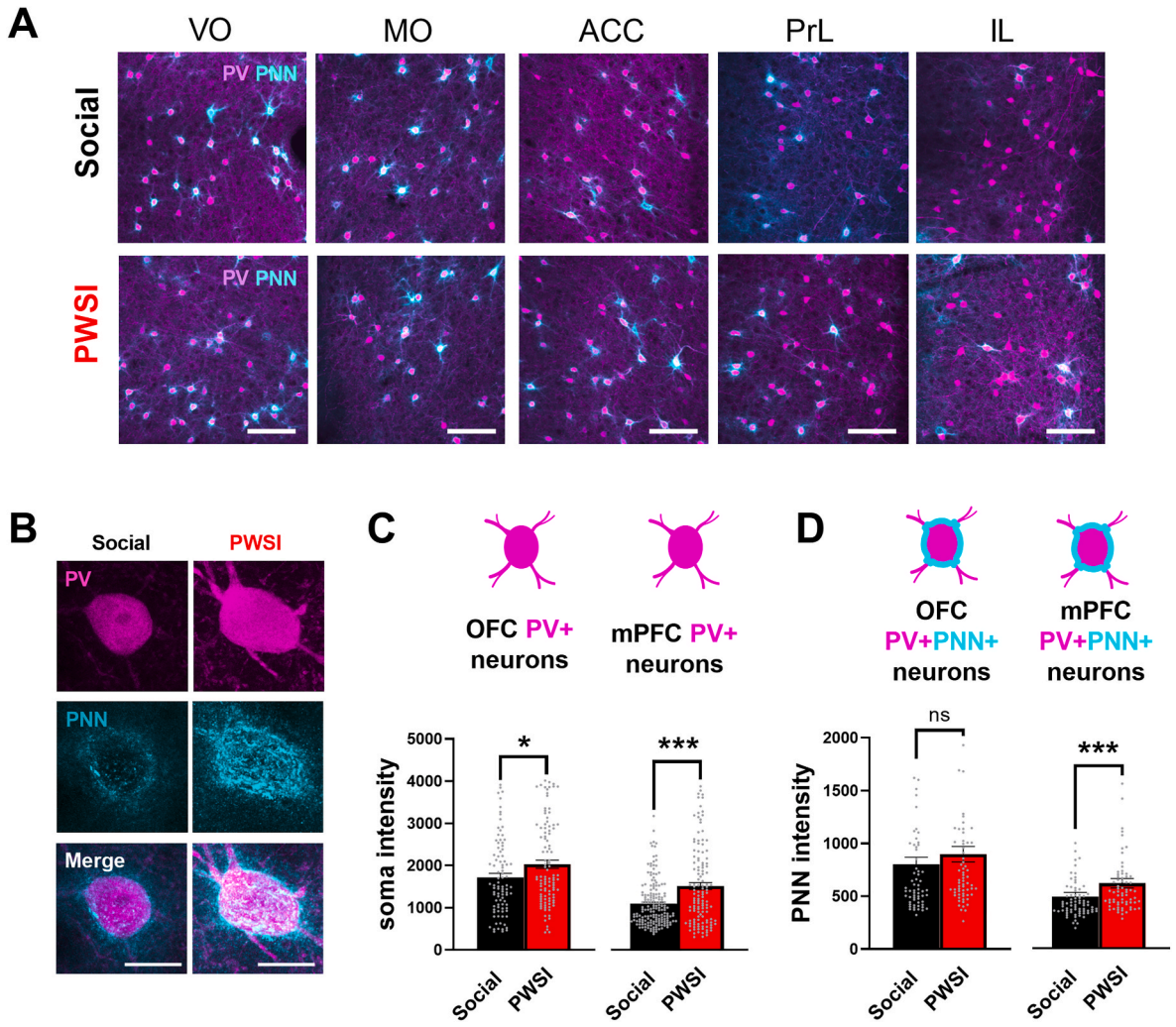

Fig. 3. PWSI increased PV and PNN intensities in the mPFC. *A*, Representative confocal maximal intensity projection images showing subregion-specific differences in the density of neurons co-labeled with PV (magenta) and WFA (PNN, cyan) in the VO, MO, ACC, PrL and IL from social and PWSI mice, respectively. Density of PV+PNN+ neurons increased in ACC and PrL compared to the ventrally located IL. Scale bar, 150 μm. *B-D, PWSI induced increased PV and PNN intensities in the mPFC. B*, Representative high resolution confocal images of PV+PNN+ neurons in the mPFC showing increased PV and PNN intensities in PWSI mice compared to social mice. Scale bar, 20 μm. *C*, Graphs showing PV soma intensities of PV neurons (OFC, n = 92 neurons from 4 social mice and n = 106 neurons from 4 PWSI mice; mPFC, n = 176 neurons from 4 social mice and n = 127 neurons from 4 PWSI mice). *D*, Graphs showing the PNN intensities of PV+PNN+ neurons (OFC, n = 63 neurons from 4 social mice and n = 68 neurons from 4 PWSI mice; mPFC, n = 75 neurons from 4 social mice and n = 70 neurons from 4 PWSI mice). All data are represented as mean ± SEM. *p < 0.05, **p < 0.01, ***p < 0.001. ACC, anterior cingulate cortex; IL, infralimbic cortex; MO, medial orbitofrontal cortex, mPFC, medial prefrontal cortex; OFC, orbitofrontal cortex; PNN, perineuronal net, PrL, prelimbic cortex, PV, parvalbumin; VO, ventral orbitofrontal cortex. (For interpretation of the references to color in this figure legend, the reader is referred to the Web version of this article.)

(Supplementary Fig. S2I). During training, large reward preference gradually increased in both PWSI and social groups (no group differences, data not shown). Introducing the delay in large reward delivery increased the preference for the small reward in both groups ($F(7, 259) = 39.845$, $p < 0.001$, Supplementary Fig. S2J), but PWSI did not affect large reward preference ($F(1, 37) = 1.829$, $p = 0.184$; Supplementary Fig. S2J). However, we observed a slight but significant decrease in the number of total responses ($F(1, 37) = 5.286$, $p = 0.027$; Supplementary Fig. S2K) suggesting a reduced motivational state in PWSI mice.

To further outline motivational and reward-related changes of PWSI, mice were subjected to the SPT (Supplementary Fig. S2L). While PWSI did not affect water consumption ($F(1, 36) = 0.520$, $p = 0.476$; data not shown) or sucrose preference ($F(1, 36) = 1.777$, $p = 0.191$; Supplementary Fig. S2M), there was a slight but significant decrease in sucrose consumption ($F(1, 36) = 4.157$, $p = 0.049$; Supplementary Fig. S2N). This, coupled with the decreased number of total responses in the delay discounting test might indicate a lowered reward value for sucrose in PWSI mice.

Overall, the above results indicate that PWSI selectively induces marked social deficits in multiple paradigms, with a slight indication towards additional motivational or reward-related disturbances.

3.3. PWSI-induced abnormal aggression is associated with subregion-specific neuronal hyperactivation in the mPFC and disrupted co-activation patterns across mPFC and OFC subregions

To investigate the impact of PWSI on the neuronal activation of PFC coupled with abnormal aggression, mice were perfused 90 min after aggressive interaction (**AGGR**) (Fig. 3A) or under baseline - resting - conditions (**BASE**), followed by c-Fos (a surrogate of neuronal activity) immunostaining. AGGR increased c-Fos expression in the OFC and mPFC compared to BASE groups (OFC: $F(1, 35) = 19.935$, $p < 0.001$, Fig. 2B, Suppl. Fig. S3A and **S3C–F**; mPFC: $F(1, 35) = 80.786$, $p < 0.001$, Fig. 2C, Suppl. Fig. S3B and **S3C–F**). Interestingly, aggressive interaction induced neuronal hyperactivation within the mPFC of PWSI mice compared to social mice (housing × AGGR interaction, $F(1, 35) = 5.414$,

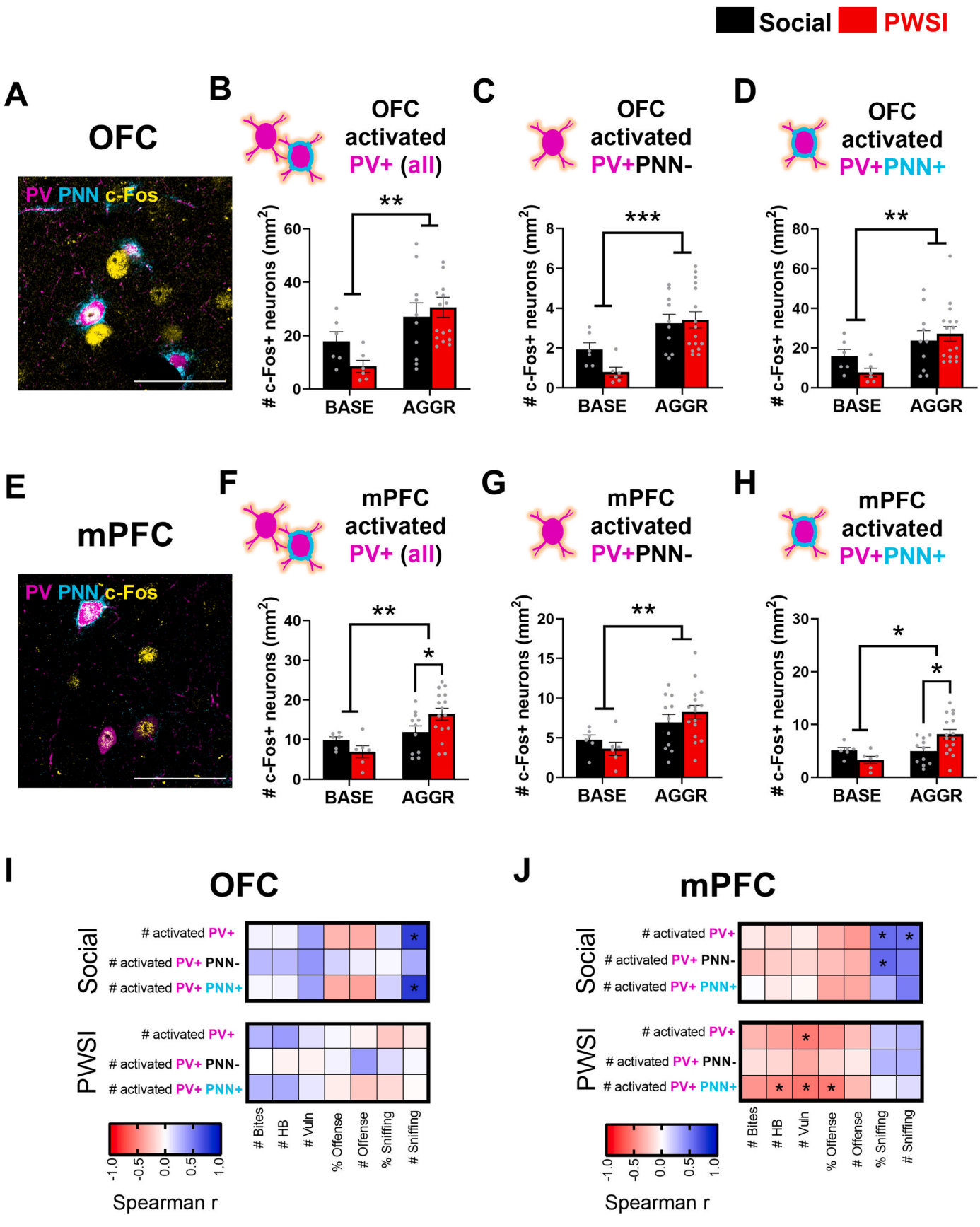

(caption on next page)

Fig. 4. PWSI-induced abnormal aggression correlates with mPFC-specific heightened activity of PV+PNN+ neurons. For the experimental timeline see Fig. 2A. *A-D, Aggressive interaction increased the activity of PV + neurons in the OFC. A*, Representative single plane confocal image showing activated (c-Fos-immunpositive, yellow) parvalbumin neurons (parvalbumin-immunpositive, magenta) surrounded by PNNs (stained with WFA, cyan) from the OFC of a PWSI mouse. *B*, Aggressive interaction (AGGR) increased the number of activated PV+ neurons compared to baseline, i.e. resting controls (BASE). Graphs show the density of activated parvalbumin neurons (PV+cFos+ double immunopositive) in the OFC. *C-D,* Aggressive interaction increased the activation of both PV+PNN- (*C)* and PV+PNN+ (*D)* neuronal populations in the OFC of social and PWSI mice. *E-H, PWSI induced hyperactivation of PV+ neurons in the mPFC following aggressive interaction. E*, Representative single plane confocal image showing activated (c-Fos+, yellow) parvalbumin neurons (PV+, magenta) with (stained with WFA, cyan) and without PNNs from the mPFC of a PWSI mouse. *F*, Aggressive interaction-specific significant increase in the density of activated PV+ neurons (PV+cFos+, double immunopositive) in the mPFC of PWSI mice compared to social mice. *G-H,* The density of activated PV+PNN- neurons (*G)* and PV+PNN+ neurons (*H)* in the mPFC revealed a PWSI-specific hyperactivation of PV+PNN+ neurons. *I-J, PWSI altered correlations between behavioral variables during aggressive interaction and activation patterns of distinct PV+ neuronal populations in the PFC. I,* Spearman correlation matrices for social mice (upper panel) and PWSI mice (lower panel) showing relationships between OFC PV+ neuron activation and behavior during AGGR. *J*, Spearman correlation matrices for social mice (upper panel) and PWSI mice (lower panel) showing relationships between mPFC PV + neuron activation and behavior during AGGR. Each square shows the Spearman's correlation coefficient as calculated by correlating mean densities of activated PV+ neurons, PV+PNN- neurons or PV+PNN+ neurons with hallmark aggression features shown in Fig. 1. Colors indicate Spearman correlation coefficients, and labels within squares correspond to p values of correlations. All data are represented as mean ± SEM. *$p < 0.05$, **$p < 0.01$, ***$p < 0.005$, AGGR, aggressive interaction; BASE, baseline i.e. resting conditions; mPFC, medial prefrontal cortex; OFC, orbitofrontal cortex; PV, parvalbumin; PV+PNN-, parvalbumin neurons without perineuronal nets; PV+PNN+, parvalbumin neurons with perineuronal nets. (For interpretation of the references to color in this figure legend, the reader is referred to the Web version of this article.)

p = 0.026; PWSI AGGR vs social AGGR, p = 0.033, Fig. 2C, Suppl. Figs. S3E and S3F). Our detailed analysis indicated that AGGR-induced neuronal hyperactivation in PWSI mice was present in all mPFC subregions (PWSI AGGR vs social AGGR; ACC p = 0.033; PrL p = 0.0257; IL p = 0.014, Suppl. Fig. S3B) suggesting an overall increase at the neuronal activation level in the mPFC of PWSI mice following a social challenge.

Our findings that aggressive interaction leads to the activation of gene expression in multiple prefrontal subregions prompted us to analyze functional connectivity by computing covariance across subjects to decipher interactions between subregions. To achieve this, we first calculated a complete set of interregional correlations in the groups of mice from each experimental group, using the results of c-Fos densities shown in Suppl. Figs. S3A and S3B. Subsequently, on the basis of these matrices, we generated network graphs for each experimental group where the nodes represent brain regions and the width of connections between nodes indicate the strength of correlation coefficients. Fig. 2D and E shows matrices that display interregional correlations for the number of c-Fos-positive cells at baseline condition in social and PWSI mice, respectively. Inspired by other studies using c-Fos as a measure of functional connectivity (Cruces-Solis et al., 2020; Salvatore et al., 2018), we considered this an exploratory approach to gain insight into the basic interregional co-activation across the experimental groups. Differences in co-activation under baseline conditions indicate that PSWI caused an altered resting state pattern (Fig. 2D and E). Upon aggressive interaction, we observed a shifted co-activation pattern in social mice compared to baseline conditions (Fig. 2D and F). Interestingly, in PWSI mice following aggressive interaction a *disrupted* co-activation pattern could be observed, as all the investigated PFC subregions exhibited correlated activity with all other regions, suggesting a PWSI-induced robust shift in PFC co-activation patterns (Fig. 2E, F and 2G). Taken together, we found that PWSI-induced abnormal aggression was paired with mPFC-specific neuronal hyperactivation along with a disrupted network co-activation state.

3.4. PWSI increased PV and PNN intensities in the mPFC

Since PV+ neurons in the PFC play key roles in maintaining synaptic excitatory/inhibitory balance during social behavior (Yizhar et al., 2011; Bicks et al., 2020) and are affected by early life adversity (Schiavone et al., 2009; Bicks et al., 2020), we examined their density in the PFC of PWSI mice and social mice (Suppl. Fig. S4A). Analyses of the OFC (Suppl. Fig. S4B) and mPFC (Suppl. Fig. S4C) subregions revealed that the density of PV+ neurons shows subregion-specific differences, but the densities are not affected by PWSI (housing F(1, 37) = 0.473, p = 0.496; subregion F(4, 146) = 10.55, p < 0.001, Fig. 3A and Suppl. Fig. S4D). Since many PV+ interneurons are enwrapped by specialized extracellular matrix assemblies named perineuronal nets (PNNs) (Suppl. Fig. S4A) (Celio et al., 1998; Härtig et al., 1999), which are highly involved in plasticity and activity of PV+ neurons (Balmer et al., 2009; Lensjø et al., 2017b), we further assessed PNN+ and PNN- PV+ neuronal densities across PFC subregions. WFA, a plant-based lectin stain that is commonly used to label PNNs (Härtig et al., 1992; Ueno et al., 2017b), was used along with PV immunolabeling to visualize PNNs around PV+ cells in the brain (Sorg et al., 2016). In the mPFC, we observed a density increase of PV+PNN+ neurons in the dorsal (ACC, PrL) subregions compared to the ventrally located IL (F(4, 146) = 120.6, p < 0.001; all pairwise comparisons p < 0.001, Fig. 3A and Suppl. Fig. S4F), and this shift was paralleled by a concomitant decrease in densities of PV+PNN- neurons (F(4, 146) = 135.1, p < 0.001; all pairwise comparisons p < 0.001, Fig. 3A and Suppl. Fig. S4E). In agreement with previous studies (Castillo-Gómez et al., 2017; Ueno et al., 2017a), we found that PWSI did not affect the overall density of neither PV+PNN+ neurons (F(1, 37) = 0.074, p = 0.788), nor PV+PNN- neurons (F(1, 37) = 0.74,8 p = 0.393, Suppl. Fig. S4E-F).

Earlier, the presence of PNNs has been reported to correlate directly with the expression of PV (Ohira et al., 2013; Yamada et al., 2015), which is an indicator of cellular activity (Donato et al., 2013). In addition, exposure to adverse experiences has been linked to aberrant PV soma and PNN intensities in the PFC (Ueno et al., 2017a; Spijker et al., 2020). Therefore, using high resolution confocal microscopy, we investigated how PWSI affects PV soma and PNN intensities of PV+ neurons and PV+PNN+ neurons, respectively. We observed that OFC and mPFC PV+ neurons in PWSI mice had significantly greater PV soma intensity (OFC, U = 3992, p = 0.028; mPFC, U = 8612, p < 0.001, Fig. 3B and C) compared with social mice. Intriguingly, this neuronal population also showed greater PNN intensity in PWSI mice (U = 1663, p < 0.001, Fig. 3B and D). This change was specific to the mPFC, as no significant differences in the intensity of PNN was observed between groups in the OFC (U = 1788, p = 0.078, Fig. 3B and D).

3.5. PWSI-induced abnormal aggression correlates with mPFC-specific heightened activity of PV+PNN+ neurons

Next, we asked whether the increased PV soma intensity and PNN intensities coincide with higher recruitment ratio of PV neurons. Thus, we performed multiple staining for c-Fos, PV, and WFA in combination with confocal microscopy to assess the density of activated PV+ neurons (Fig. 4A and E). Following aggressive interaction, we observed an increased density of activated PV+ neurons (c-Fos+ PV+ neurons) in the OFC and mPFC compared to baseline conditions (OFC, F(1, 34) = 10.67, p = 0.003, Fig. 4A and B; mPFC, F(1, 35) = 10.88, p = 0.002, Fig. 4E and F). Remarkably, following aggressive interaction, we detected more activated PV+ neurons in the mPFC of PWSI mice compared to social

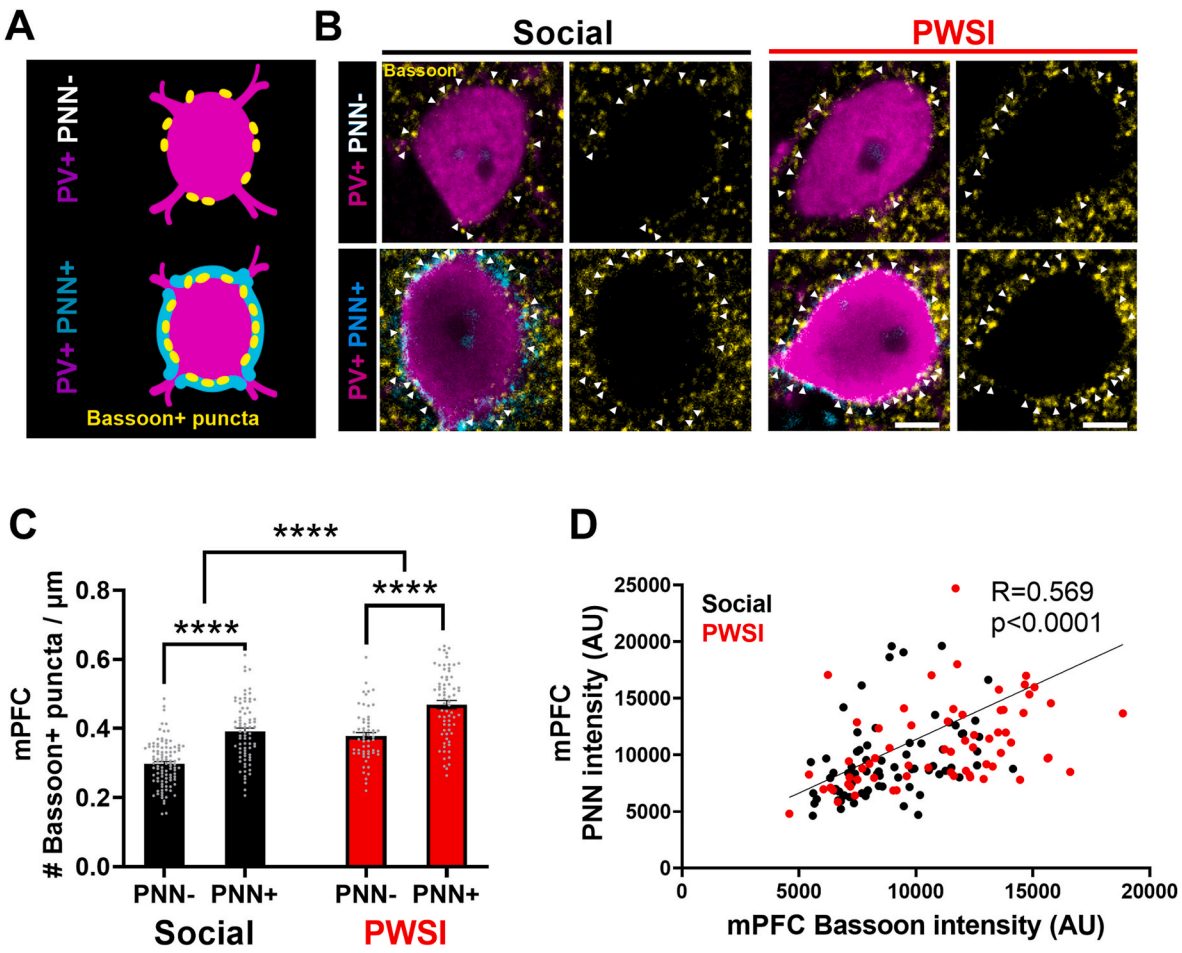

Fig. 5. PWSI increased the density of synaptic inputs opposed to the perisomatic region of PV+ neurons in the mPFC. *A,* Schematic drawings depicting parvalbumin neurons (PV+, magenta) without perineuronal net (PNN-) or with PNN (cyan, PNN+), targeted by Bassoon presynaptic release site marker immunoreactive puncta (yellow). *B,* Representative single plane confocal images showing immunoreactivity for PV (magenta) and Bassoon (yellow) as well as *Wisteria floribunda* agglutinin staining for PNNs (cyan) for a PNN- (upper panel) and a PNN+ (bottom panel) PV+ neuron within the mPFC of social and PWSI mice, respectively. White arrowheads indicate close appositions of Bassoon+ puncta surrounding the perisomatic region of PV+PNN- (top panel) and PV+PNN+ (bottom panel) neurons from the mPFC of social and PWSI mice. Scale bar, 4 µm. *C*, Bar graphs showing that PV+PNN+ neurons receive more Bassoon+ puncta densities at their perisomatic region compared to PV+PNN- neurons and PWSI caused an overall increase in the density of Bassoon+ puncta at the perisomatic region of PV+ neurons (n = 101 PNN- neurons and n = 75 PNN+ neurons from 4 social mice; n = 57 PNN- neurons and n = 70 PNN+ neurons from 4 PWSI mice). *D*, Scatter plots with regression lines represent a significant positive correlation of the perisomatic PNN intensity and perisomatic Bassoon intensity of PV+ neurons. The inset shows Spearman's correlation coefficient (R). All data are represented as mean ± SEM. ****p < 0.0001. mPFC, medial prefrontal cortex. (For interpretation of the references to color in this figure legend, the reader is referred to the Web version of this article.)

mice (interaction: F(1, 35) = 4.568, p = 0.030, social AGGR vs PWSI AGGR, p = 0.027, Fig. 4F). No such changes were apparent at the level of OFC (F(1, 34) = 1.858, p = 0.188, Fig. 4B).

We sought to determine whether the presence of PNNs modulates PV+ neuronal activation during aggressive interaction, by investigating how fighting relates to the density of activated PV+PNN- neurons (PV+PNN-cFos+) and activated PV+PNN+ neurons (PV+PNN+cFos+). Throughout the PFC, both PV+PNN- neurons (OFC, F(1, 34) = 16.975, p = 0.001, Fig. 4C; mPFC, F(1, 35) = 10.594, p = 0.003, Fig. 4G) and PV+PNN+ neurons (OFC, F(1, 34) = 8.955, p = 0.005, Fig. 4D; mPFC, F (1, 35) = 5.702, p = 0.022, Fig. 4H) of the aggressive interaction groups displayed an elevation in activation compared to baseline groups. Upon fighting, PWSI animals showed an increased density of activated PV+PNN+ neurons in the mPFC compared to social mice (interaction, F (1, 35) = 6.5961, p = 0.0146, Fig. 4H) which might imply that PV+PNN+ neurons may contribute to the observed behavioral deficits induced by PWSI.

To gain further insight into the relationship between the activation ratios of PV+ neuron subpopulations and behavioral outcome, we computed correlations between the density of activated PV+, PV+PNN+, PV+PNN- subpopulations and key features of aggressive or social behaviors (Fig. 4I and J). In social mice, the ratio of activated PV+ neurons within the OFC and mPFC showed a positive correlation with non-aggressive social sniffing, thereby confirming PV+ neuron engagement during social interaction. Intriguingly, social sniffing did not correlate with the activation of PV+ neurons in PWSI mice, however, PWSI resulted in significant, negative correlation between multiple aggression-related behavioral parameters and the activation of PV+ neurons, most robustly with PV+PNN+ neurons.

Overall, the above results suggest that the activity of PV+ neurons surrounded by PNN may directly or indirectly contribute to abnormal aggression induced by early social adversities.

3.6. PWSI increased the density of synaptic inputs surrounding the perisomatic region of PV+ neurons in the mPFC

In agreement with previous reports establishing a role of PNNs in the organization and stability of the synaptic circuitry (Fig. 5A) (Favuzzi et al., 2017; Lensjø et al., 2017a; Carceller et al., 2020), we detected more Bassoon immunoreactive (Bassoon+, presynaptic release site

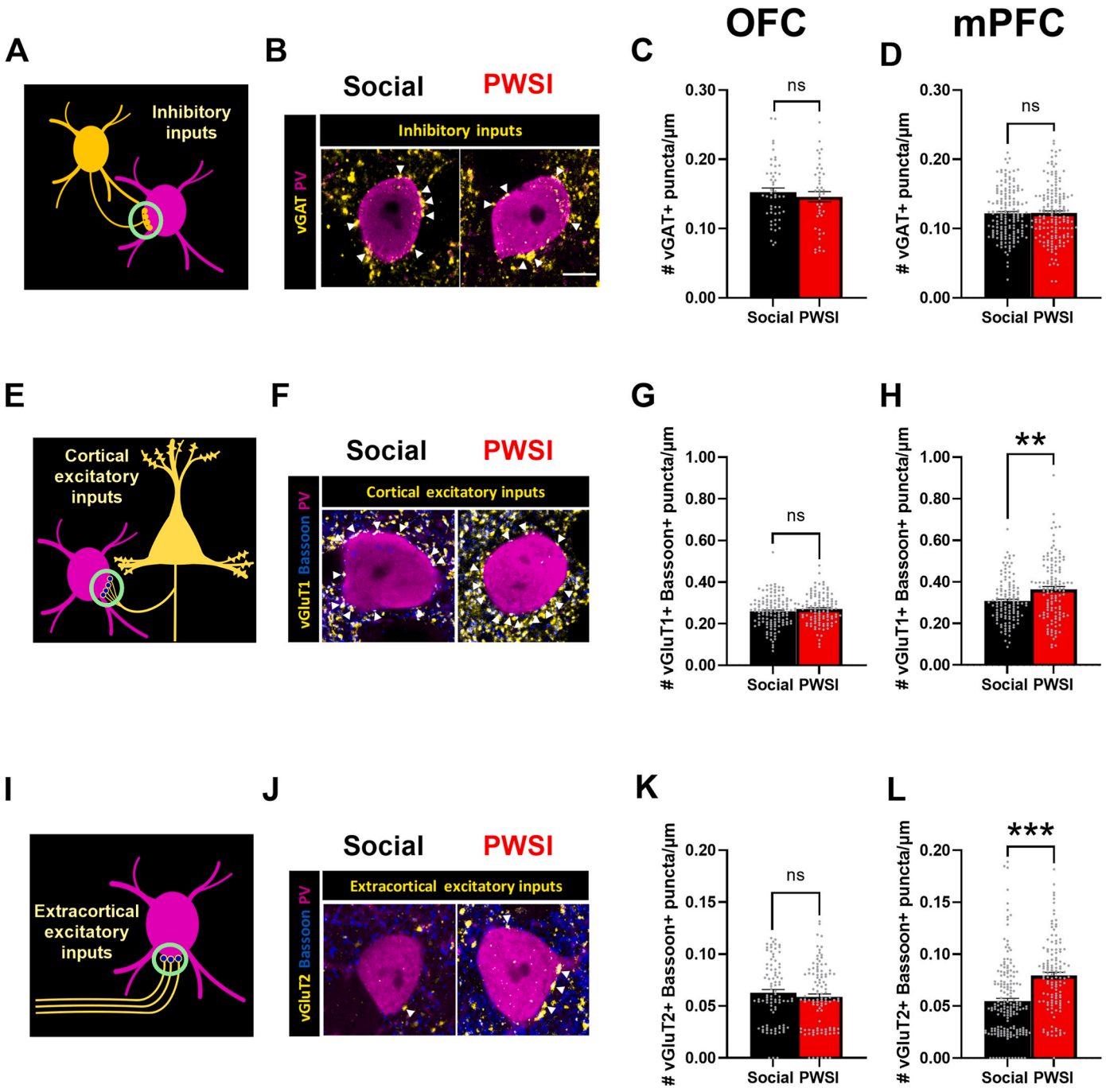

(caption on next page)

Fig. 6. PWSI increased the density of excitatory cortical (vGluT1+) and subcortical (vGluT2+) inputs impinging on the perisomatic region of PV+ neurons in the mPFC. *A*, Schematic drawing showing a local inhibitory neuron (yellow) targeting the perisomatic region of a PV+ neuron (magenta). Yellow circles indicate the vesicular GABA transporter (vGAT+) immunoreactive synapses analyzed in this experiment. *B*, Representative single plane confocal images showing close appositions of vGAT + puncta (white arrowheads) surrounding a PV + neuron (magenta) from the mPFC of social and PWSI mice. Scale bar, 5 μm. *C-D PWSI did not affect the density of inhibitory inputs targeting the perisomatic region of PV + neurons*. Bar graphs showing the density of vGAT+ puncta targeting the perisomatic region of PV+ neurons from the OFC (*C*) and mPFC (*D*), respectively (OFC, n = 50 neurons from 4 social mice and n = 42 neurons from 4 PWSI mice; mPFC, n = 163 neurons from 4 social mice and n = 162 neurons from 4 PWSI mice). *E-L, PWSI increased the density of excitatory inputs targeting the perisomatic region of PV + neurons in the mPFC. E,* Schematic drawing showing a local putative pyramidal neuron (yellow) targeting the perisomatic region of a PV+ neuron (magenta). Yellow circles indicate the vesicular glutamate transporter type 1 (vGluT1+) immunoreactive synapses coupled with blue dots signaling Bassoon immunoreactive presynaptic active zones analyzed in this experiment. *F*, Representative single plane confocal images showing close appositions of vGluT1+Bassoon+ puncta (white arrowheads) surrounding a PV+ neuron from the mPFC of social and PWSI mice. Same magnification as in *B*. Bar graphs showing the density of vGluT1+Bassoon+ puncta targeting the perisomatic region of PV+ neurons from the OFC (*G*) and mPFC (*H*), respectively (OFC, n = 129 neurons from 4 social mice and n = 109 neurons from 4 PWSI mice; mPFC, n = 121 neurons from 4 social mice and n = 128 neurons from 4 PWSI mice). *I*, Schematic drawing showing extracortical excitatory inputs (yellow) targeting the perisomatic region of a PV+ neuron (magenta). Yellow circles indicate vesicular glutamate transporter type 2 (vGluT2+) immunoreactive synapses with blue dots signaling Bassoon immunoreactive presynaptic active zones analyzed in this experiment. *J,* Representative single plane confocal images showing close appositions of vGluT2+Bassoon+ puncta (white arrowheads) surrounding a PV+ neuron from the mPFC of social and PWSI mice. Similar magnification as in *B*. Bar graphs showing the density of vGluT2+Bassoon+ puncta targeting the perisomatic region of PV+ neurons from the OFC (*K*) and mPFC (*L*), respectively (OFC, n = 92 neurons from 4 social mice and n = 106 neurons from 4 PWSI mice; mPFC, n = 176 neurons from 4 social mice and n = 127 neurons from 4 PWSI mice). All data are represented as mean ± SEM. ***p < 0.0001. mPFC, medial prefrontal cortex; OFC, orbitofrontal cortex; vGAT, vesicular GABA transporter; vGluT1, vesicular glutamate transporter type 1; vGluT2, vesicular glutamate transporter type 2. (For interpretation of the references to color in this figure legend, the reader is referred to the Web version of this article.)

marker) (Dani et al., 2010) puncta at the perisomatic region of PV+PNN+ neurons versus PV+PNN- neurons ($F(1, 299) = 91.87$, $p < 0.001$, Fig. 5B and C). Along with this, we detected higher perisomatic Bassoon+ fluorescence intensities surrounding PV+PNN+ neurons in both social and PWSI groups ($F(1, 299) = 9.264$, $p = 0.003$). Noteworthy, independently of PNN coverage, PWSI caused an overall increase in the density of Bassoon+ puncta surrounding the somata of PV+ neurons ($F(1, 299) = 68.33$, $p < 0.001$, Fig. 5C). In the case of PV+PNN+ neurons, we also observed a strong positive correlation between PNN fluorescence intensity and perisomatic Bassoon+ fluorescence intensity (Spearman $r = 0.5688$, $p < 0.0001$, Fig. 5D) corroborating previous findings from the visual cortex and the hippocampus indicating that PNNs play an essential role in the maintenance of synaptic stability (Dityatev et al., 2010; Lensjø et al., 2017a).

3.7. PWSI increased the density of excitatory cortical (vGluT1+) and subcortical (vGluT2+) boutons impinging on the perisomatic region of PV+ neurons

Since early-life adversity can affect the density of inhibitory synapses (McKlveen et al., 2019), we tested whether PWSI affected the density of vesicular GABA transporter (vGAT+) immunoreactive inputs targeting the perisomatic region of PV+ neurons. PWSI did not affect the density of inhibitory inputs (OFC, $t(90) = 0.693$, $p = 0.490$; mPFC, $t(323) = 0.16$, $p = 0.873$ Fig. 6A–D).

Excitatory synaptic input can control the deposition of PNNs around PV+ interneurons (Dityatev et al., 2007; Devienne et al., 2021). Since we found that PWSI leads to an increase in the recruitment of PV+ neurons following aggressive interaction (Fig. 4), and the PNNs' staining intensity also increased around PV+ neurons (Fig. 3D), we asked whether PWSI affected the excitatory synaptic drive impinging on the perisomatic region of PV+ neurons. Thus, we studied the excitatory glutamatergic inputs targeting the somata of cortical PV+ interneurons: intracortical (Fig. 6E-H) and subcortical inputs (Fig. 6I-L) which use presynaptic vesicular glutamate transporter 1 (vGluT1) and 2 (vGluT2), respectively (Takamori et al., 2000, 2001; Fremeau et al., 2001). We applied multiple labeling immunostaining and confocal microscopy to assess the density of vGluT1 immunoreactive (vGluT1+) and vGluT2 immunoreactive (vGluT2+) synaptic puncta apposing the somata of PV+ neurons in combination with the presynaptic release site marker Bassoon+ (Fig. 6F and J). We observed a significant increase in the density of both cortical and subcortical inputs surrounding the somata of PV+ neurons in the mPFC of PWSI mice compared to social mice (vGluT1+Basson+ puncta, $U = 5945$, $p < 0.002$, Fig. 6H; vGluT2+Basson+ puncta, $U = 6455$, $p < 0.001$; Fig. 6L). The observed increase in the excitatory drive was specific for the mPFC since no such changes were detectable at the level of the OFC (vGluT1+Basson+ puncta, $U = 6450$, $p = 0.273$, Fig. 6G; vGluT2+Basson+ puncta, $U = 4445$, $p = 0.273$, Fig. 6K). These data tentatively suggest that aggressive interaction-associated recruitment of PV+ neurons in PWSI mice could have been caused by enhanced excitatory drive arising from both cortical and subcortical sources.

3.8. PWSI increased the density of excitatory inputs targeting PV+ neurons in the mPFC, regardless of the presence of PNN

Next, we asked whether the observed PWSI-evoked synaptic imbalances in mPFC PV+ neurons occur in a PNN-dependent manner. Consistently with previous observations (Carceller et al., 2020), PV+PNN+ neurons received more vGAT+ inputs compared to PV+PNN- neurons ($F(1, 310) = 11.46$, $p < 0.001$, Fig. 7A and D). In line with this, we also observed increased perisomatic vGAT fluorescence intensity around PV+PNN+ neurons ($F(1, 311) = 10.62$, $p = 0.001$), however, PWSI had no effect on the density of inhibitory inputs ($F(1, 310) = 0.054$, $p = 0.823$, Fig. 7A and D). In addition, we observed that the PNN intensities of PV+ neurons positively correlated with perisomatic vGAT+ puncta intensities ($r = 0.768$, $p < 0.001$, data not shown). In the case of cortical excitatory inputs, we observed that PV+PNN+ neurons received higher densities of vGluT1+Bassoon+ inputs relative to PV+PNN- neurons ($F(1, 240) = 8.884$, $p = 0.003$, Fig. 7B and E). PWSI resulted in higher densities of vGluT1+ Bassoon+ inputs targeting mPFC PV+ neurons in the PWSI mice ($F(1, 240) = 12.14$, $p < 0.0001$, Fig. 7B and E), which did not depend on PNN coverage and housing interaction, $F(1, 240) = 1.143$, $p = 0.286$). We did not observe any difference in the intensity of vGluT1+ staining (all p values > 0.05, data not shown). We also observed that the PNN intensities of PV+ neurons positively correlated with perisomatic vGluT1+ puncta intensities ($r = 0.6182$, $p < 0.0001$, data not shown).

In the case of subcortical excitatory inputs, we detected higher vGluT2+ Bassoon+ puncta densities in the perisomatic regions of PV+PNN+ neurons compared to the PV+PNN- population ($F(1, 299) = 12.36$, $p < 0.001$, Fig. 7C and F). Similarly to cortical excitatory inputs, the observed significant increase in the densities of vGluT2+Bassoon+ inputs of PWSI mice relative to social mice ($F(1, 299) = 29.94$, $p < 0.001$, Fig. 7C and F) did not depend on PNN coverage (PNN and housing interaction, $F(1, 299) = 0.005$, $p = 0.941$). We also found that the PNN intensities of PV+ neurons positively correlated with perisomatic vGluT2+ puncta intensities ($r = 0.2425$, $p < 0.003$, data not shown) suggesting that PNNs may play a role in the stabilization of subcortical inputs (Faini et al., 2018) in the mPFC.

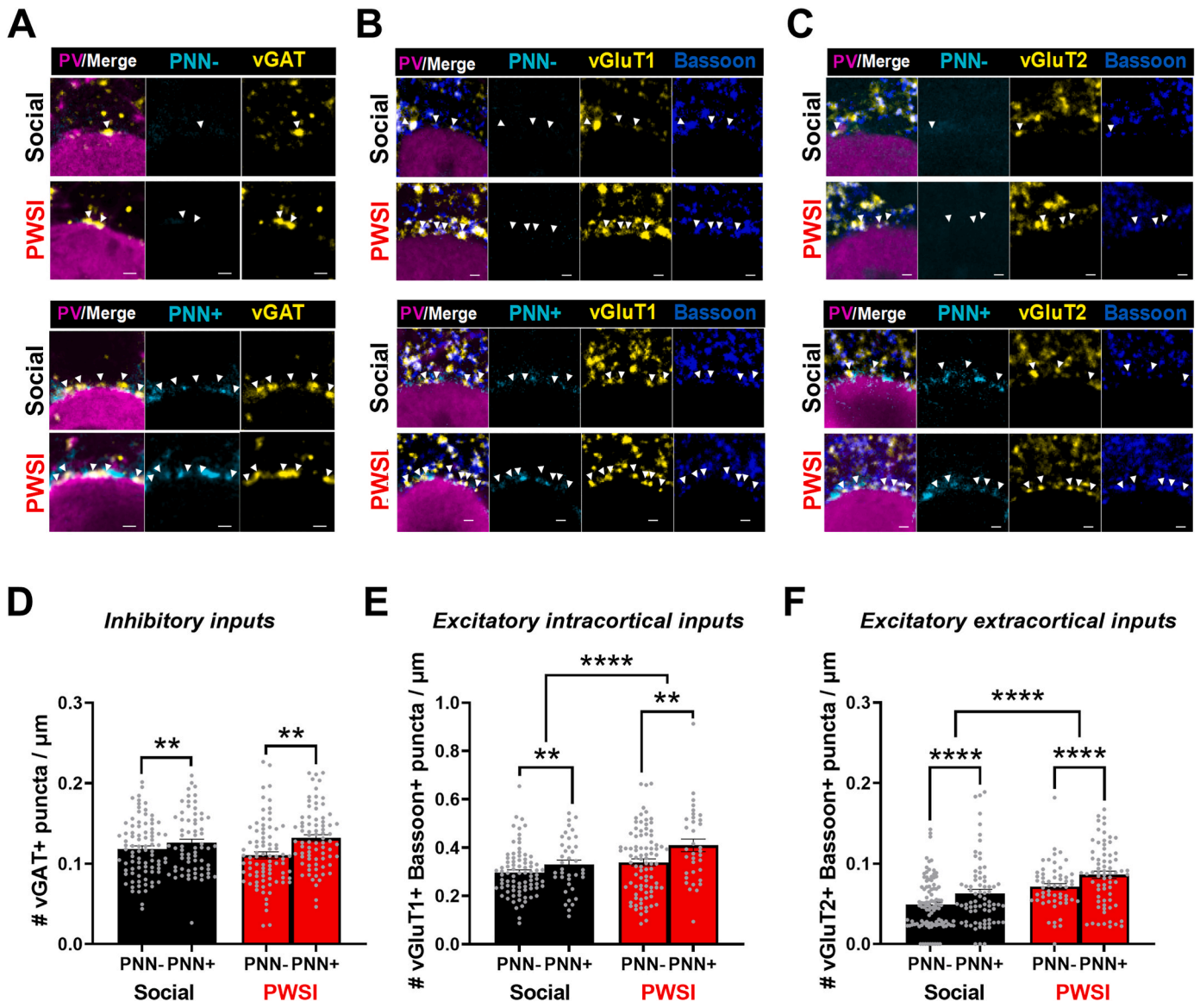

Fig. 7. PWSI increased the density of perisomatic excitatory inputs targeting PV+ neurons in the mPFC, regardless of the presence of PNN. *A and D, PV + PNN+ neurons receive more inhibitory inputs than PV+PNN- neurons in both social and PWSI mice. A*, Representative single plane confocal images showing immunoreactivity for PV (magenta) and vGAT (yellow) as well as *Wisteria floribunda* agglutinin staining for PNNs (cyan) for a PNN- (top panel) and a PNN+ (bottom panel) PV+ neuron from the mPFC of social and PWSI mice, respectively. White arrowheads indicate vGAT+ puncta. Scale bar, 1 µm. *D*, Bar graphs showing the density of vGAT+ puncta targeting the perisomatic region of PV+PNN- and PV+PNN+ neurons in the mPFC (n = 87 PV+PNN- and n = 67 PV+PNN+ neurons from 4 social mice and n = 83 PV+PNN- and n = 77 PV+PNN+ neurons from 4 PWSI mice). *B, C, E, and F, PWSI increased the density of intracortical and extracortical excitatory inputs targeting the perisomatic region of PV + neurons and the presence of PNN is associated with higher densities of excitatory inputs. B,* Representative single plane confocal images showing immunoreactivity for PV (magenta), vGluT1 (yellow) and Bassoon (blue) as well as *Wisteria floribunda* agglutinin staining for PNNs (cyan) for a PNN- (top panel) and a PNN+ (bottom panel) PV+ neuron from the mPFC of social and PWSI mice, respectively. White arrowheads indicate vGluT1+Bassoon+ puncta. Scale bar, 1 µm. *E*, Bar graphs showing the density of vGluT1+Bassoon+ puncta targeting the perisomatic region of PV+PNN- and PV+PNN+ neurons in the mPFC (n = 83 PV+PNN- and n = 38 PV+PNN+ neurons from 4 social mice and n = 88 PV+PNN- and n = 34 PV+PNN+ neurons from 4 PWSI mice). *C,* Representative single plane confocal images showing immunoreactivity for PV (magenta), vGluT2 (yellow) and Bassoon (blue) as well as *Wisteria floribunda* agglutinin staining for PNNs (cyan) for a PNN- (top panel) and a PNN+ (bottom panel) PV+ neuron from the mPFC of social and PWSI mice, respectively. White arrowheads indicate vGluT2+Bassoon+ puncta. Scale bar, 1 µm. *F*, Bar graphs showing the density of vGluT2+Bassoon+ puncta targeting the perisomatic region of PV+PNN- and PV+PNN+ neurons in the mPFC (n = 101 PV+PNN- and n = 75 PV+PNN+ neurons from 4 social mice and n = 57 PV+PNN- and n = 70 PV+PNN+ neurons from 4 PWSI mice). All data are represented as mean ± SEM. *p < 0.05, **p < 0.01, ***p < 0.005. PNN, perineuronal net; PV, parvalbumin; vGAT, vesicular GABA transporter; vGluT1, vesicular glutamate transporter type 1; vGluT2, vesicular glutamate transporter type 2. (For interpretation of the references to color in this figure legend, the reader is referred to the Web version of this article.)

3.9. PWSI reduced the density of PV+ inhibitory boutons (baskets) targeting the perisomatic compartment of pyramidal cells in the mPFC

PV+ basket interneurons constitute one of the main sources of perisomatic inhibition onto excitatory neurons (Fig. 8A), providing a synchronized modulation of cortical activity through the regulation of oscillations (Freund and Katona, 2007; Kubota, 2014). In order to investigate whether PWSI affected the output features of PV+ interneurons, we assessed the vesicular GABA transporter (vGAT+) immunoreactive inhibitory synapses of PV+ basket interneurons impinging onto the soma of pyramidal cells in layer 5 of mPFC, identified by Kv2.1 immunoreactivity (Fig. 8E) (Vereczki et al., 2016).

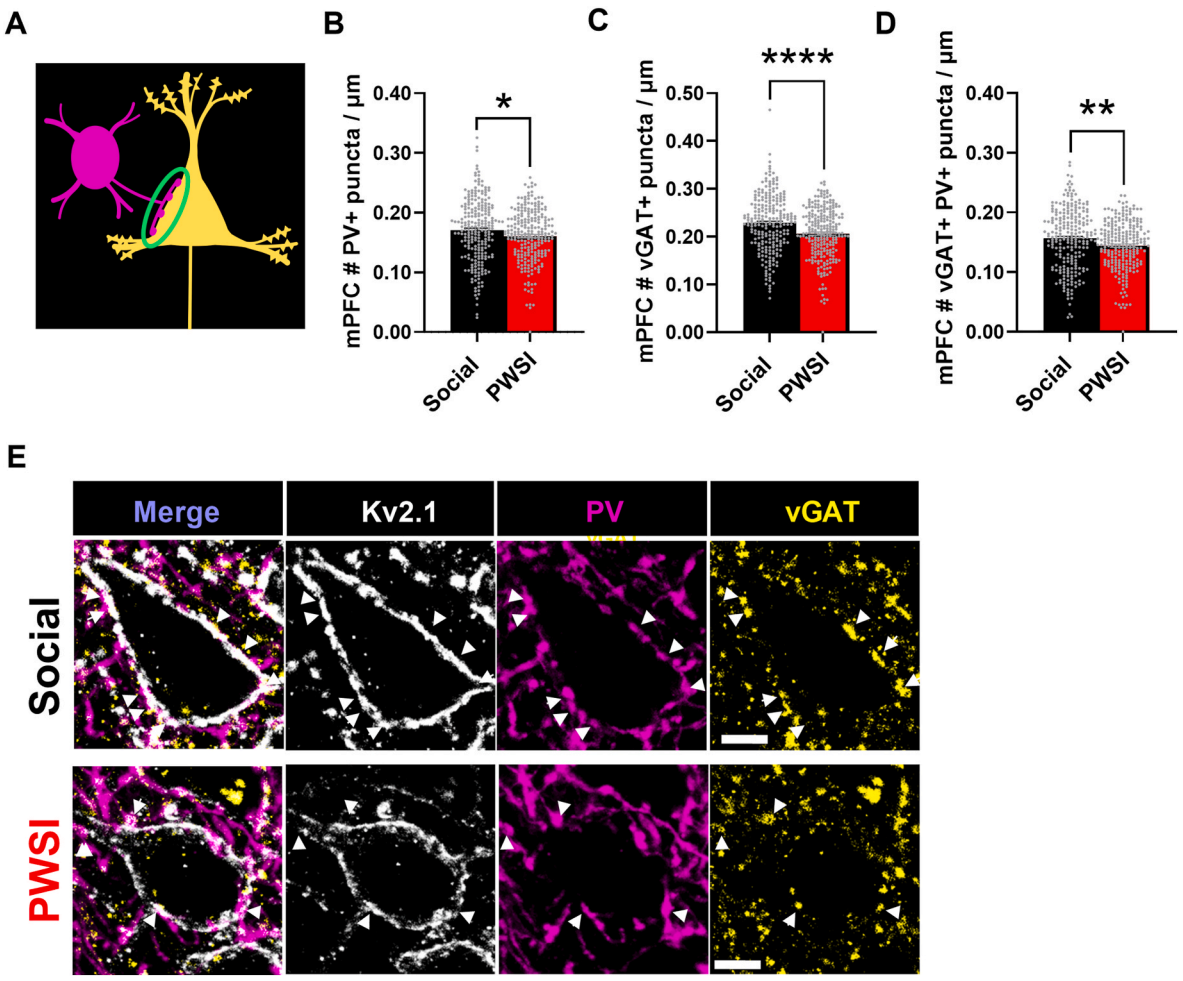

Fig. 8. PWSI reduced the density of PV+ inhibitory boutons (baskets) targeting the perisomatic compartment of pyramidal cells in the mPFC. *A*, Schematic drawing depicting the inhibitory axons of PV+ neurons (magenta) targeting the perisomatic region of a pyramidal neuron (yellow) forming PV immunoreactive basket-like innervation. *B-E*, *PWSI reduced the inhibitory output of PV + neurons*. Bar graphs showing the density of PV+ puncta (*B*), vGAT+ puncta (*C*), and vGAT+PV+ puncta (*D*) targeting the perisomatic region of putative pyramidal neurons (n = 239 neurons from 4 social mice and n = 243 neurons from 4 PWSI mice). *E*, Representative single plane confocal images from the mPFC showing immunoreactivity for PV (magenta) and vGAT (yellow) as well as voltage-gated potassium channel type 2.1 (Kv2.1, white, labels the perisomatic membrane of neurons) for social (top panel) and PWSI (bottom panel) mice, respectively. White arrowheads indicate vGAT+PV+ puncta opposing the perisomatic compartment of putative pyramidal neurons. Scale bar, 1 µm. All data are represented as mean ± SEM. *p < 0.05, **p < 0.01, ***p < 0.005. (For interpretation of the references to color in this figure legend, the reader is referred to the Web version of this article.)

Overall, we detected fewer vGAT+ puncta ($t(480) = 4.272$, $p < 0.001$, Fig. 8C) and PV+ puncta ($t(480) = 2.268$, $p = 0.024$, Fig. 8B) around pyramidal neurons of PWSI mice. mPFC layer 5 (L5) pyramidal cells in PWSI mice received fewer inhibitory inputs from PV+ neurons, as we observed a reduction in the density of PV+vGAT+ surrounding Kv2.1 immunoreactive pyramidal neuron somata ($t(480) = 2.895$, $p = 0.004$, Fig. 8D and E). Together, these data show that PV+ inhibitory synaptic inputs to L5 pyramidal cells are severely reduced after PWSI, suggesting less effective perisomatic inhibition in the mPFC, which might contribute to the observed hyperactivation of the mPFC (Fig. 2C and Suppl. Fig. S3B).

4. Discussion

Here we report prefrontal cortical network dysfunction underlying abnormal aggressive behavior that results from early social neglect in a preclinical rodent model.

Studies have shown that PWSI leads to increased aggression in male mice and rats (Tóth et al., 2008; Koike et al., 2009; Biro et al., 2017; Li et al., 2022), but this study is the first to present a detailed analysis including quantitative and qualitative aspects of aggression in male mice. We chose to use male mice only since female mice display lower levels of aggression in general (Trainor et al., 2010; Hashikawa et al., 2017). However, future studies are needed to elucidate whether abnormal aggression or other forms of social disturbances (e.g. behavioral fragmentation) are present in female PWSI mice too.

Our research identifies species-atypical abnormal social patterns in PWSI male mice, and we demonstrate that these are not limited to aggression, describing other key disturbances including behavioral fragmentation (i.e. abnormal rapid switching between social behavioral elements), increased defensive behavior and the robust appearance of excessive social vigilance, a characteristic behavior of PWSI mice that has not been investigated or described previously in this paradigm, even though hypervigilance to threat and negative attention bias have often been cited as a consequence of early-life maltreatment in human studies (Gibb et al., 2009; Troller-Renfree et al., 2015). PWSI leads to endocrine and autonomic arousal in rats (Toth et al., 2011), and clinical studies also highlight neglect-induced changes in stress-reactivity (Koss et al., 2014; Peng et al., 2014), providing a possible background for hyperarousal involving the social opponent. Behavioral fragmentation implicates an inability to recognize social cues and deliver context-adequate responses, the parallels of which can also be seen in PWSI rats (Tóth

et al., 2008) and humans that have experienced childhood maltreatment (Keil and Price, 2009; Kay and Green, 2016), revealing ubiquitous social aberrations caused by early-life adverse experiences.

In the delay discounting test, PWSI mice showed a decreased number of total responses compared to social mice. This, coupled with the decreased sucrose consumption in the sucrose preference test, potentially implies that the inherent reward value of sucrose is reduced in PWSI mice. Indeed, a study of PWSI rats has shown dulled sensitivity to sucrose in isolated rats (Wukitsch et al., 2020).

Contrarily to the robust, consistent appearance of social disturbances across various PWSI studies, the existence of non-social anxiety varies highly over PWSI research. Whereas some studies show that PWSI mice display increased anxiety and fear responses (Koike et al., 2009; Liu et al., 2015), behavioral disturbances highlighted by our multi-domain test battery were mainly exclusive to the social domain. A plausible explanation is that some isolation-induced behavioral effects are strain- and test-specific or otherwise depend heavily on the population that was investigated (Võikar et al., 2004).

At the network level, we found increased neuronal activation of the PFC in social mice following aggressive behavior, confirming previous findings in rats and humans (Toth et al., 2012; Biro et al., 2017; Cupaioli et al., 2021; Takahashi, 2022). Additionally, in PWSI mice we observed even greater densities of active neurons following aggressive interaction, which were specific to mPFC subregions, as no such changes were found in the OFC. These data reproduced our previous findings in rats submitted to PWSI (Toth et al., 2012; Biro et al., 2017).

Based on the marked behavioral phenotype induced by PWSI and on neuronal tracing reports reporting that the PFC exhibits high interconnectivity between its various subregions (Ährlund-Richter et al., 2019), here we also aimed to assess functional connectivity patterns across PFC subregions via c-Fos activity (Cruces-Solis et al., 2020; Salvatore et al., 2018). Using our c-Fos dataset, we calculated correlational matrices between prefrontal subregions to decipher interactions across the mPFC and observed altered correlation patterns following aggressive interaction, implicating the existence of finely balanced network operations between prefrontal subregions during normal agonistic interactions. In contrast, in the PFC of PWSI mice we found that neuronal activation across all subregions correlated with each other. It is a plausible explanation that mPFC-specific neuronal hyperactivation heavily impacts brain-wide network operations, thus contributing to the disrupted co-activation profile seen in PWSI mice.

In this study we found that, in both social and PWSI mice, following aggressive interaction PV+ neurons showed marked c-Fos activation in both the OFC and the mPFC, possibly reflecting a general increase in network activity and thus an elevation in the recruitment of PV+ neurons. Accordingly, recent studies employing fiber photometry and electrophysiological recordings indicate an activity-increase of mPFC PV+ neurons during social encounters (Bicks et al., 2020). Interestingly, we observed that following fighting an even greater elevated density of activated PV+ neurons in the mPFC of PWSI mice could be observed compared to social mice, lending additional support for the argument that maladaptive developmental programming of PV+ neurons might contribute to social behavioral deficits in adulthood. Indeed, at the cellular level, we found an increase in the intensities of WFA-labeled PNNs surrounding PV+ neurons in the mPFC of PWSI mice, suggesting altered plasticity of PV+ cells, since PNNs have been known to regulate synaptic and cellular plasticity of this neuron population (Sorg et al., 2016).

Whereas the appearance of PNNs coincides with the maturation of PV+ neurons and a concomitant decrease in their plasticity, the removal of PNNs promotes plasticity within cortical regions (Balmer et al., 2009), proposing that PWSI might render PV+PNN+ neurons into a more rigid state (Donato et al., 2013). Moreover, we uncovered an increase in the density of activated PV+PNN+, but not PV+PNN- neurons in the mPFC of abnormally aggressive PWSI mice. This also raises the possibility that PV+PNN+ neurons, compared to PV+PNN- neurons, might be more deeply embedded in the mPFC microcircuitry and thus play a pronounced role in circuit operations related to agonistic behaviors. Indeed, in PWSI mice the activity of PV+PNN+ neurons negatively correlated with hallmark features of aggressive behavior including the number of attack bites and vulnerable area-targeting bites, and time spent with offensive behavior. On the other hand, in social mice, prefrontal PV+ neuronal activity – mostly involving the PV+PNN- population – positively correlates with non-aggressive sniffing behavior. This suggests that different PV+ subpopulations may adjust individual behavioral responses during social challenges.

Noteworthy, in PWSI mice, these changes were specific to the mPFC compared to the OFC, proposing that early-life adversity results in region-specific alterations within frontal cortical regions. The overall activity changes in PV+ neuronal populations suggest a dysregulated inhibitory tone within the mPFC, which might contribute to the observed network disturbances and neuronal hyperactivation. We must note that our results do not exclude the possibility that abnormal hyperactivation of the PWSI mPFC is not specific to social challenges and more studies are needed to verify a potential selectivity or lack thereof.

Previous studies pinpointed that PV+ neuronal function highly depends on their synaptic inputs (Donato et al., 2013). To investigate how PWSI may affect the synaptic inputs of PV+PNN- and PV+PNN+ neurons in the PFC, we compared the density of perisomatic puncta expressing different synaptic markers labeling GABAergic inhibitory synapses (vGAT+), glutamatergic cortical (vGluT1+), and glutamatergic extra-cortical (vGluT2+) synapses, respectively. PV+ neurons receive by far the most excitatory glutamatergic inputs compared to other interneuron populations (Gulyás et al., 1999) and PV+ neuron-specific changes in glutamatergic neurotransmission are implicated in neurodevelopmental disorders (Rotaru et al., 2012) and in aggression-regulation (Mikics et al., 2018; Newman et al., 2018; Guyon et al., 2021). In our study, PWSI increased the density of both vGluT1+ and vGluT2+ inputs targeting the somata of mPFC PV+ neurons. PV+PNN+ neurons received higher densities of both vGluT1+ and vGluT2+ inputs compared to PV+PNN- neurons. Based on this one could argue that abnormal aggressive behavior coupled with higher overall mPFC activity involved the recruitment of PV+PNN+ neurons, which was exacerbated by an enhanced excitatory drive emanating from both cortical and subcortical sources, respectively.

Here we first show that PWSI caused a remarkable increase of vGluT2+ extra-cortical inputs indicating a strong thalamic involvement of PV+ neurons, particularly regarding PV+PNN+ neurons. Indeed, calretinin expressing paraventricular thalamic (PVT) and vGluT2-expressing mediodorsal thalamic (MD) neurons heavily innervate the mPFC (Mátyás et al., 2018; Gao et al., 2020) and the mPFC PV+ neurons, respectively (Hur and Zaborszky, 2005; Delevich et al., 2015; Mukherjee et al., 2021). A recent report implicated that early life stress could affect the structural and functional maturation of PVT neurons (Kooiker et al., 2021). Thus, one might not exclude the possibility that in our study PWSI might have affected the mPFC-projecting thalamic axons, leading to increased vGluT2+ densities around PV+ neurons. PWSI did not affect the inhibitory neurotransmission at the somata of PV+ neurons as we did not detect changes in the perisomatic vGAT+ puncta densities between the experimental groups.

Taken together, we found that in PWSI mice aggressive interaction led to an increased PV+ neuronal activation that co-occurred with enhanced glutamatergic drive on the perisomatic domain of PV+ neurons. Our results provide support for the claim that early life adversity perturbs the programming of glutamatergic neurotransmission at PV+ neurons in the mPFC.

Since PV+ interneurons constitute one of the main sources of perisomatic inhibition onto excitatory pyramidal neurons, providing a synchronized modulation of cortical activity through the regulation of oscillations (Freund and Katona, 2007; Kubota, 2014), we measured vGAT+PV+ inhibitory puncta impinging onto the soma of pyramidal

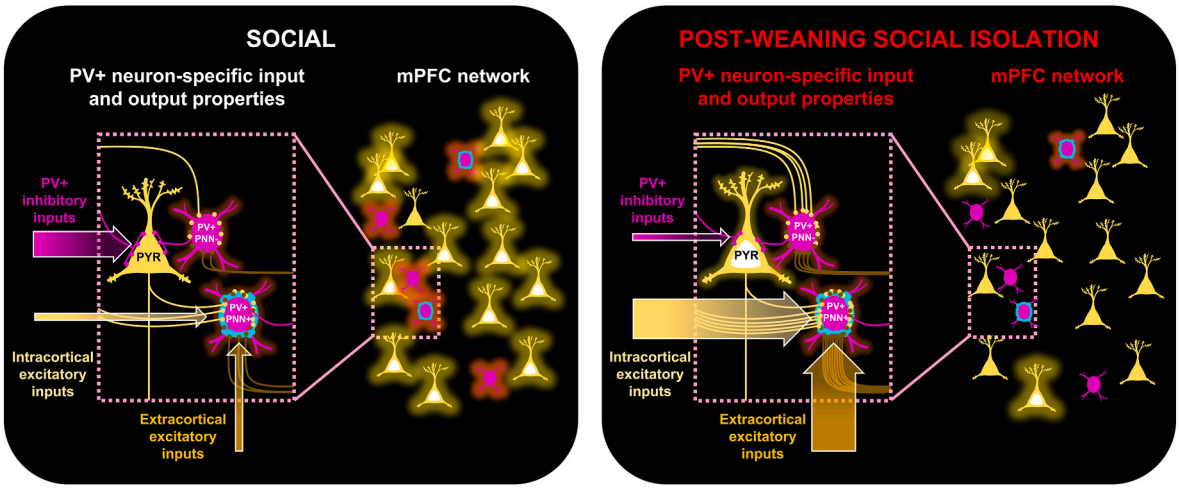

Fig. 9. Summary of PWSI-induced changes in the mPFC. *At the network level*, in response to a social challenge PWSI mice show a general hyperactivation of the mPFC and a shifted co-activation pattern between mPFC subregions compared to social mice, depicted here by the differing patterns of activated (glowing) neurons in social and PWSI mice. *At the cellular level*, PWSI increased the overall density of synaptic inputs surrounding the perisomatic region of PV+ neurons, including cortical excitatory (vGluT1+, light gold color) and extracortical excitatory (vGluT2+, dark gold) inputs. The increase in excitatory inputs surrounding PV+ interneurons did not depend on PNN-coverage. PWSI also reduced the density of PV+ inhibitory boutons (magenta) targeting the perisomatic compartment of pyramidal cells in the mPFC. (For interpretation of the references to color in this figure legend, the reader is referred to the Web version of this article.)

cells in the mPFC. We observed a marked reduction in the inhibitory output of PV+ interneurons, characterized by a reduced number of inhibitory puncta surrounding mPFC L5 pyramidal neurons, suggesting less effective perisomatic inhibiton in the mPFC, which might contribute to the observed hyperactivation of the mPFC (Fig. 9). It is interesting to consider that the increased excitatory drive arriving onto PV+ cells could have emerged as a compensatory mechanism for the decreased PV+ neuron-mediated inhibition of mPFC layer 5 pyramidal neurons. Assuming this was true, the prefrontal functional connectivity analyses indicate that while a precarious E/I balance can be maintained under baseline conditions, the network is unable to selectively adjust to more complex tasks demanding high levels of cognitive control, e.g. a social challenge, as shown by hyperactivation of the mPFC in PWSI mice subjected to the resident-intruder test.

5. Conclusion

Our findings indicate that early life social adversity results in a disrupted network organization in the mPFC in adulthood along with social deficits and abnormal aggression. The data presented here further indicate that PNNs and both input and output traits of PV+ neurons are affected by PWSI and that these changes may participate in altering neuronal network operations underlying agonistic social interactions (Fig. 9). Elucidating such mechanisms is paramount in the identification of novel targets, allowing the development of cell-specific interventions in the treatment of early-life maltreatment-induced mental diseases associated with excessive aggression.

Funding

This study was supported by the Hungarian Brain Research Program (NAP 2.0) [grant number 2017–1.2.1-NKP-2017-00002]; by the National Research, Development and Innovation Office (NKFIH) [grant number K125390]; by the Eötvös Loránd Research Network (ELKH) [grant number SA-49/2021]; and by the National Laboratory of Translational Neuroscience (TINL) [grant number RRF-2.3.1-21-2022-00011].

CRediT authorship contribution statement

Laszlo Biro: Conceptualization, Methodology, Formal analysis, Investigation, Data curation, Writing – original draft, Writing – review & editing, Visualization, Supervision. **Christina Miskolczi:** Conceptualization, Methodology, Formal analysis, Investigation, Writing – original draft, Writing – review & editing, Visualization. **Huba Szebik:** Software, Investigation, Data curation. **Biborka Bruzsik:** Investigation. **Zoltan Kristof Varga:** Formal analysis, Data curation, Writing – review & editing. **Laszlo Szente:** Investigation. **Mate Toth:** Conceptualization, Methodology, Writing – original draft. **Jozsef Halasz:** Conceptualization, Methodology, Formal analysis, Writing – original draft. **Eva Mikics:** Conceptualization, Methodology, Formal analysis, Writing – original draft, Writing – review & editing, Visualization, Supervision, Project administration, Funding acquisition.

Declaration of competing interest

The authors declare the following financial interests/personal relationships which may be considered as potential competing interests: Eva Mikics reports financial support was provided by Hungarian Brain Research Program. Eva Mikics reports financial support was provided by National Research, Development and Innovation Office (NKFIH). Eva Mikics reports financial support was provided by National Laboratory of Translational Neuroscience.

Data availability

Data will be made available on request.

Acknowledgments

We thank Dr. Manó Aliczki for his help in the design of the delay discounting tests. We thank all the core facilities of our institute for their supportive help: the Behavioral Studies Unit for help with behavioral testing (Dr. Kornel Demeter), the Nikon Microscopy Center for help with microscopy (Dr. Laszlo Barna and Dr. Csaba Pongor) and the Medical Gene Technology Unit for help with mouse breeding.

Appendix A. Supplementary data

Supplementary data to this article can be found online at https://doi.org/10.1016/j.ynstr.2023.100546.

References

Adriani, W., Caprioli, A., Granstrem, O., Carli, M., Laviola, G., 2003. The spontaneously hypertensive-rat as an animal model of ADHD: evidence for impulsive and non-impulsive subpopulations. Neurosci. Biobehav. Rev. 27, 639–651. https://doi.org/10.1016/j.neubiorev.2003.08.007.

Ährlund-Richter, S., Xuan, Y., van Lunteren, J.A., Kim, H., Ortiz, C., Pollak Dorocic, I., Meletis, K., Carlén, M., 2019. A whole-brain atlas of monosynaptic input targeting four different cell types in the medial prefrontal cortex of the mouse. Nat. Neurosci. 22, 657–668. https://doi.org/10.1038/s41593-019-0354-y.

Aliczki, M., Fodor, A., Balogh, Z., Haller, J., Zelena, D., 2014. The effects of lactation on impulsive behavior in vasopressin-deficient Brattleboro rats. Horm. Behav. 66, 545–551. https://doi.org/10.1016/j.yhbeh.2014.08.002.

Balmer, T.S., Carels, V.M., Frisch, J.L., Nick, T.A., 2009. Modulation of perineuronal nets and parvalbumin with developmental song learning. J. Neurosci. 29, 12878–12885. https://doi.org/10.1523/JNEUROSCI.2974-09.2009.

Benjamini, Y., Hochberg, Y., 1995. Controlling the false discovery rate: a practical and powerful approach to multiple testing. J. Roy. Stat. Soc. B 57, 289–300. https://doi.org/10.1111/j.2517-6161.1995.tb02031.x.

Bicks, L.K., Yamamuro, K., Flanigan, M.E., Kim, J.M., Kato, D., Lucas, E.K., Koike, H., Peng, M.S., Brady, D.M., Chandrasekaran, S., Norman, K.J., Smith, M.R., Clem, R.L., Russo, S.J., Akbarian, S., Morishita, H., 2020. Prefrontal parvalbumin interneurons require juvenile social experience to establish adult social behavior. Nat. Commun. 11, 1003. https://doi.org/10.1038/s41467-020-14740-z.

Birnie, M.T., Kooiker, C.L., Short, A.K., Bolton, J.L., Chen, Y., Baram, T.Z., 2020. Plasticity of the reward circuitry after early-life adversity: mechanisms and significance. Biol. Psychiatr. 87, 875–884. https://doi.org/10.1016/j.biopsych.2019.12.018.

Biro, L., Sipos, E., Bruzsik, B., Farkas, I., Zelena, D., Balazsfi, D., Toth, M., Haller, J., 2018. Task division within the prefrontal cortex: distinct neuron populations selectively control different aspects of aggressive behavior via the hypothalamus. J. Neurosci. 38, 4065–4075. https://doi.org/10.1523/JNEUROSCI.3234-17.2018.

Biro, L., Toth, M., Sipos, E., Bruzsik, B., Tulogdi, A., Bendahan, S., Sandi, C., Haller, J., 2017. Structural and functional alterations in the prefrontal cortex after post-weaning social isolation: relationship with species-typical and deviant aggression. Brain Struct. Funct. 222, 1861–1875. https://doi.org/10.1007/s00429-016-1312-z.

Blakemore, S.-J., 2008. The social brain in adolescence. Nat. Rev. Neurosci. 9, 267–277. https://doi.org/10.1038/nrn2353.

Cabungcal, J.-H., Steullet, P., Morishita, H., Kraftsik, R., Cuenod, M., Hensch, T.K., Do, K. Q., 2013. Perineuronal nets protect fast-spiking interneurons against oxidative stress. Proc. Natl. Acad. Sci. U.S.A. 110, 9130–9135. https://doi.org/10.1073/pnas.1300454110.

Carceller, H., Guirado, R., Ripolles-Campos, E., Teruel-Marti, V., Nacher, J., 2020. Perineuronal nets regulate the inhibitory perisomatic input onto parvalbumin interneurons and γ activity in the prefrontal cortex. J. Neurosci. 40, 5008–5018. https://doi.org/10.1523/JNEUROSCI.0291-20.2020.

Carr, C.P., Martins, C.M.S., Stingel, A.M., Lemgruber, V.B., Juruena, M.F., 2013. The role of early life stress in adult psychiatric disorders: a systematic review according to childhood trauma subtypes. J. Nerv. Ment. Dis. 201, 1007–1020. https://doi.org/10.1097/NMD.0000000000000049.

Carulli, D., Verhaagen, J., 2021. An extracellular perspective on CNS maturation: perineuronal nets and the control of plasticity. Int. J. Mol. Sci. 22, 2434. https://doi.org/10.3390/ijms22052434.

Castillo-Gómez, E., Pérez-Rando, M., Bellés, M., Gilabert-Juan, J., Llorens, J.V., Carceller, H., Bueno-Fernández, C., García-Mompó, C., Ripoll-Martínez, B., Curto, Y., Sebastiá-Ortega, N., Moltó, M.D., Sanjuan, J., Nacher, J., 2017. Early social isolation stress and perinatal NMDA receptor antagonist treatment induce changes in the structure and neurochemistry of inhibitory neurons of the adult amygdala and prefrontal cortex. eneuro 4. https://doi.org/10.1523/ENEURO.0034-17.2017. ENEURO.0034-17.2017.

Celio, M.R., Spreafico, R., De Biasi, S., Vitellaro-Zuccarello, L., 1998. Perineuronal nets: past and present. Trends Neurosci. 21, 510–515. https://doi.org/10.1016/S0166-2236(98)01298-3.

Courtin, J., Chaudun, F., Rozeske, R.R., Karalis, N., Gonzalez-Campo, C., Wurtz, H., Abdi, A., Baufreton, J., Bienvenu, T.C.M., Herry, C., 2014. Prefrontal parvalbumin interneurons shape neuronal activity to drive fear expression. Nature 505, 92–96. https://doi.org/10.1038/nature12755.

Cruces-Solis, H., Nissen, W., Ferger, B., Arban, R., 2020. Whole-brain signatures of functional connectivity after bidirectional modulation of the dopaminergic system in mice. Neuropharmacology 178, 108246. https://doi.org/10.1016/j.neuropharm.2020.108246.

Cupaioli, F.A., Zucca, F.A., Caporale, C., Lesch, K.-P., Passamonti, L., Zecca, L., 2021. The neurobiology of human aggressive behavior: neuroimaging, genetic, and neurochemical aspects. Prog. Neuro-Psychopharmacol. Biol. Psychiatry 106, 110059. https://doi.org/10.1016/j.pnpbp.2020.110059.

Dalley, J.W., Mar, A.C., Economidou, D., Robbins, T.W., 2008. Neurobehavioral mechanisms of impulsivity: fronto-striatal systems and functional neurochemistry. Pharmacol. Biochem. Behav. 90, 250–260. https://doi.org/10.1016/j.pbb.2007.12.021.

Dani, A., Huang, B., Bergan, J., Dulac, C., Zhuang, X., 2010. Superresolution imaging of chemical synapses in the brain. Neuron 68, 843–856. https://doi.org/10.1016/j.neuron.2010.11.021.

de Almeida, R., 2002. Aggression escalated by social instigation or by discontinuation of reinforcement ("Frustration") in mice inhibition by anpirtoline: a 5-HT1B receptor agonist. Neuropsychopharmacology 27, 171–181. https://doi.org/10.1016/S0893-133X(02)00291-9.

Delevich, K., Tucciarone, J., Huang, Z.J., Li, B., 2015. The mediodorsal thalamus drives feedforward inhibition in the anterior cingulate cortex via parvalbumin interneurons. J. Neurosci. 35, 5743–5753. https://doi.org/10.1523/JNEUROSCI.4565-14.2015.

Devienne, G., Picaud, S., Cohen, I., Piquet, J., Tricoire, L., Testa, D., Di Nardo, A.A., Rossier, J., Cauli, B., Lambolez, B., 2021. Regulation of perineuronal nets in the adult cortex by the activity of the cortical network. J. Neurosci. 41, 5779–5790. https://doi.org/10.1523/JNEUROSCI.0434-21.2021.

Dityatev, A., Brückner, G., Dityateva, G., Grosche, J., Kleene, R., Schachner, M., 2007. Activity-dependent formation and functions of chondroitin sulfate-rich extracellular matrix of perineuronal nets. Dev. Neurobiol. 67, 570–588. https://doi.org/10.1002/dneu.20361.

Dityatev, A., Schachner, M., Sonderegger, P., 2010. The dual role of the extracellular matrix in synaptic plasticity and homeostasis. Nat. Rev. Neurosci. 11, 735–746. https://doi.org/10.1038/nrn2898.

Donato, F., Rompani, S.B., Caroni, P., 2013. Parvalbumin-expressing basket-cell network plasticity induced by experience regulates adult learning. Nature 504, 272–276. https://doi.org/10.1038/nature12866.

Duque-Wilckens, N., Steinman, M.Q., Busnelli, M., Chini, B., Yokoyama, S., Pham, M., Laredo, S.A., Hao, R., Perkeybile, A.M., Minie, V.A., Tan, P.B., Bales, K.L., Trainor, B. C., 2018. Oxytocin receptors in the anteromedial bed nucleus of the stria terminalis promote stress-induced social avoidance in female California mice. Biol. Psychiatr. 83, 203–213. https://doi.org/10.1016/j.biopsych.2017.08.024.

Faini, G., Aguirre, A., Landi, S., Lamers, D., Pizzorusso, T., Ratto, G.M., Deleuze, C., Bacci, A., 2018. Perineuronal nets control visual input via thalamic recruitment of cortical PV interneurons. Elife 7, e41520. https://doi.org/10.7554/eLife.41520.

Favuzzi, E., Marques-Smith, A., Deogracias, R., Winterflood, C.M., Sánchez-Aguilera, A., Mantoan, L., Maeso, P., Fernandes, C., Ewers, H., Rico, B., 2017. Activity-dependent gating of parvalbumin interneuron function by the perineuronal net protein brevican. Neuron 95, 639–655. https://doi.org/10.1016/j.neuron.2017.06.028 e10.

Fremeau, R.T., Troyer, M.D., Pahner, I., Nygaard, G.O., Tran, C.H., Reimer, R.J., Bellocchio, E.E., Fortin, D., Storm-Mathisen, J., Edwards, R.H., 2001. The expression of vesicular glutamate transporters defines two classes of excitatory synapse. Neuron 31, 247–260. https://doi.org/10.1016/S0896-6273(01)00344-0.

Freund, T.F., Katona, I., 2007. Perisomatic inhibition. Neuron 56, 33–42. https://doi.org/10.1016/j.neuron.2007.09.012.

Gao, C., Leng, Y., Ma, J., Rooke, V., Rodriguez-Gonzalez, S., Ramakrishnan, C., Deisseroth, K., Penzo, M.A., 2020. Two genetically, anatomically and functionally distinct cell types segregate across anteroposterior axis of paraventricular thalamus. Nat. Neurosci. 23, 217–228. https://doi.org/10.1038/s41593-019-0572-3.

Gibb, B.E., Schofield, C.A., Coles, M.E., 2009. Reported history of childhood abuse and young adults' information-processing biases for facial displays of emotion. Child. Maltreat. 14, 148–156. https://doi.org/10.1177/1077559508326358.

Gilbert, R., Widom, C.S., Browne, K., Fergusson, D., Webb, E., Janson, S., 2009. Burden and consequences of child maltreatment in high-income countries. Lancet 373, 68–81. https://doi.org/10.1016/S0140-6736(08)61706-7.

Guirado, R., Carceller, H., Castillo-Gómez, E., Castrén, E., Nacher, J., 2018. Automated analysis of images for molecular quantification in immunohistochemistry. Heliyon 4, e00669. https://doi.org/10.1016/j.heliyon.2018.e00669.

Gulyás, A.I., Megias, M., Emri, Z., Freund, T.F., 1999. Total number and ratio of excitatory and inhibitory synapses converging onto single interneurons of different types in the CA1 area of the rat Hippocampus. J. Neurosci. 19, 10082–10097. https://doi.org/10.1523/JNEUROSCI.19-22-10082.1999.

Guyon, N., Zacharias, L.R., van Lunteren, J.A., Immenschuh, J., Fuzik, J., Märtin, A., Xuan, Y., Zilberter, M., Kim, H., Meletis, K., Lopes-Aguiar, C., Carlén, M., 2021. Adult trkB signaling in parvalbumin interneurons is essential to prefrontal network dynamics. J. Neurosci. 41, 3120–3141. https://doi.org/10.1523/JNEUROSCI.1848-20.2021.

Härtig, W., Brauer, K., Brückner, G., 1992. Wisteria floribunda agglutinin-labelled nets surround parvalbumin-containing neurons. Neuroreport 3, 869. https://doi.org/10.1097/00001756-199210000-00012. –872.

Härtig, W., Derouiche, A., Welt, K., Brauer, K., Grosche, J., Mäder, M., Reichenbach, A., Brückner, G., 1999. Cortical neurons immunoreactive for the potassium channel Kv3.1b subunit are predominantly surrounded by perineuronal nets presumed as a buffering system for cations. Brain Res. 842, 15–29. https://doi.org/10.1016/S0006-8993(99)01784-9.

Hashikawa, K., Hashikawa, Y., Tremblay, R., Zhang, J., Feng, J.E., Sabol, A., Piper, W.T., Lee, H., Rudy, B., Lin, D., 2017. Esr1+ cells in the ventromedial hypothalamus control female aggression. Nat. Neurosci. 20, 1580–1590. https://doi.org/10.1038/nn.4644.

Hensch, T.K., 2004. Critical period regulation. Annu. Rev. Neurosci. 27, 549–579. https://doi.org/10.1146/annurev.neuro.27.070203.144327.

Hur, E.E., Zaborszky, L., 2005. Vglut2 afferents to the medial prefrontal and primary somatosensory cortices: a combined retrograde tracing in situ hybridization. J. Comp. Neurol. 483, 351–373. https://doi.org/10.1002/cne.20444.

Juraska, J.M., Willing, J., 2017. Pubertal onset as a critical transition for neural development and cognition. Brain Res. 1654, 87–94. https://doi.org/10.1016/j.brainres.2016.04.012.

Kay, C.L., Green, J.M., 2016. Social cognitive deficits and biases in maltreated adolescents in UK out-of-home care: relation to disinhibited attachment disorder and psychopathology. Dev. Psychopathol. 28, 73–83. https://doi.org/10.1017/S0954579415000292.

Keil, V., Price, J.M., 2009. Social information-processing patterns of maltreated children in two social domains. J. Appl. Dev. Psychol. 30, 43–52. https://doi.org/10.1016/j.appdev.2008.10.003.

Kelly, P.A., Viding, E., Wallace, G.L., Schaer, M., De Brito, S.A., Robustelli, B., McCrory, E.J., 2013. Cortical thickness, surface area, and gyrification abnormalities in children exposed to maltreatment: neural markers of vulnerability? Biol. Psychiatr. 74, 845–852. https://doi.org/10.1016/j.biopsych.2013.06.020.

Kempes, M., Matthys, W., de Vries, H., van Engeland, H., 2005. Reactive and proactive aggression in children A review of theory, findings and the relevance for child and adolescent psychiatry. Eur. Child Adolesc. Psychiatr. 14, 11–19. https://doi.org/10.1007/s00787-005-0432-4.

Kim, H., Ährlund-Richter, S., Wang, X., Deisseroth, K., Carlén, M., 2016. Prefrontal parvalbumin neurons in control of attention. Cell 164, 208–218. https://doi.org/10.1016/j.cell.2015.11.038.

Koike, H., Ibi, D., Mizoguchi, H., Nagai, T., Nitta, A., Takuma, K., Nabeshima, T., Yoneda, Y., Yamada, K., 2009. Behavioral abnormality and pharmacologic response in social isolation-reared mice. Behav. Brain Res. 202, 114–121. https://doi.org/10.1016/j.bbr.2009.03.028.

Kolk, S.M., Rakic, P., 2022. Development of prefrontal cortex. Neuropsychopharmacology 47, 41–57. https://doi.org/10.1038/s41386-021-01137-9.

Kooiker, C.L., Birnie, M.T., Baram, T.Z., 2021. The paraventricular thalamus: a potential sensor and integrator of emotionally salient early-life experiences. Front. Behav. Neurosci. 15, 673162 https://doi.org/10.3389/fnbeh.2021.673162.

Koss, K.J., Hostinar, C.E., Donzella, B., Gunnar, M.R., 2014. Social deprivation and the HPA axis in early development. Psychoneuroendocrinology 50, 1–13. https://doi.org/10.1016/j.psyneuen.2014.07.028.

Kubota, Y., 2014. Untangling GABAergic wiring in the cortical microcircuit. Curr. Opin. Neurobiol. 26, 7–14. https://doi.org/10.1016/j.conb.2013.10.003.

Larsen, B., Luna, B., 2018. Adolescence as a neurobiological critical period for the development of higher-order cognition. Neurosci. Biobehav. Rev. 94, 179–195. https://doi.org/10.1016/j.neubiorev.2018.09.005.

Lensjø, K.K., Christensen, A.C., Tennøe, S., Fyhn, M., Hafting, T., 2017a. Differential expression and cell-type specificity of perineuronal nets in Hippocampus, medial entorhinal cortex, and visual cortex examined in the rat and mouse. eneuro 4. https://doi.org/10.1523/ENEURO.0379-16.2017. ENEURO.0379-16.2017.

Lensjø, K.K., Lepperød, M.E., Dick, G., Hafting, T., Fyhn, M., 2017b. Removal of perineuronal nets unlocks juvenile plasticity through network mechanisms of decreased inhibition and increased gamma activity. J. Neurosci. 37, 1269–1283. https://doi.org/10.1523/JNEUROSCI.2504-16.2016.

Li, X., Sun, H., Zhu, Y., Wang, F., Wang, X., Han, L., Cui, D., Luo, D., Zhai, Y., Zhuo, L., Xu, X., Yang, J., Li, Y., 2022. Dysregulation of prefrontal parvalbumin interneurons leads to adult aggression induced by social isolation stress during adolescence. Front. Mol. Neurosci. 15, 1010152 https://doi.org/10.3389/fnmol.2022.1010152.

Liu, J.-H., You, Q.-L., Wei, M.-D., Wang, Q., Luo, Z.-Y., Lin, S., Huang, L., Li, S.-J., Li, X.-W., Gao, T.-M., 2015. Social isolation during adolescence strengthens retention of fear memories and facilitates induction of late-phase long-term potentiation. Mol. Neurobiol. 52, 1421–1429. https://doi.org/10.1007/s12035-014-8917-0.

Lotze, M., Veit, R., Anders, S., Birbaumer, N., 2007. Evidence for a different role of the ventral and dorsal medial prefrontal cortex for social reactive aggression: an interactive fMRI study. Neuroimage 34, 470–478. https://doi.org/10.1016/j.neuroimage.2006.09.028.

Mátyás, F., Komlósi, G., Babiczky, Á., Kocsis, K., Barthó, P., Barsy, B., Dávid, C., Kanti, V., Porrero, C., Magyar, A., Szűcs, I., Clasca, F., Acsády, L., 2018. A highly collateralized thalamic cell type with arousal-predicting activity serves as a key hub for graded state transitions in the forebrain. Nat. Neurosci. 21, 1551–1562. https://doi.org/10.1038/s41593-018-0251-9.

McKlveen, J.M., Moloney, R.D., Scheimann, J.R., Myers, B., Herman, J.P., 2019. "Braking" the prefrontal cortex: the role of glucocorticoids and interneurons in stress adaptation and pathology. Biol. Psychiatr. 86, 669–681. https://doi.org/10.1016/j.biopsych.2019.04.032.

Mikics, É., Guirado, R., Umemori, J., Tóth, M., Biró, L., Miskolczi, C., Balázsfi, D., Zelena, D., Castrén, E., Haller, J., Karpova, N.N., 2018. Social learning requires plasticity enhanced by fluoxetine through prefrontal bdnf-TrkB signaling to limit aggression induced by post-weaning social isolation. Neuropsychopharmacology 43, 235–245. https://doi.org/10.1038/npp.2017.142.

Mukherjee, A., Lam, N.H., Wimmer, R.D., Halassa, M.M., 2021. Thalamic circuits for independent control of prefrontal signal and noise. Nature 600, 100–104. https://doi.org/10.1038/s41586-021-04056-3.

Murthy, S., Kane, G.A., Katchur, N.J., Lara Mejia, P.S., Obiofuma, G., Buschman, T.J., McEwen, B.S., Gould, E., 2019. Perineuronal nets, inhibitory interneurons, and anxiety-related ventral hippocampal neuronal oscillations are altered by early life adversity. Biol. Psychiatr. 85, 1011–1020. https://doi.org/10.1016/j.biopsych.2019.02.021.

Newman, E.L., Covington, H.E., Suh, J., Bicakci, M.B., Ressler, K.J., DeBold, J.F., Miczek, K.A., 2019. Fighting females: neural and behavioral consequences of social defeat stress in female mice. Biol. Psychiatr. 86, 657–668. https://doi.org/10.1016/j.biopsych.2019.05.005.

Newman, E.L., Terunuma, M., Wang, T.L., Hewage, N., Bicakci, M.B., Moss, S.J., DeBold, J.F., Miczek, K.A., 2018. A role for prefrontal cortical NMDA receptors in murine alcohol-heightened aggression. Neuropsychopharmacology 43, 1224–1234. https://doi.org/10.1038/npp.2017.253.

Ohira, K., Takeuchi, R., Iwanaga, T., Miyakawa, T., 2013. Chronic fluoxetine treatment reduces parvalbumin expression and perineuronal nets in gamma-aminobutyric acidergic interneurons of the frontal cortex in adult mice. Mol. Brain 6, 43. https://doi.org/10.1186/1756-6606-6-43.

Peng, H., Long, Y., Li, J., Guo, Y., Wu, H., Yang, Y., Ding, Y., He, J., Ning, Y., 2014. Hypothalamic-pituitary-adrenal axis functioning and dysfunctional attitude in depressed patients with and without childhood neglect. BMC Psychiatr. 14, 45. https://doi.org/10.1186/1471-244X-14-45.

Petanjek, Z., Judaš, M., Šimić, G., Rašin, M.R., Uylings, H.B.M., Rakic, P., Kostović, I., 2011. Extraordinary neoteny of synaptic spines in the human prefrontal cortex. Proc. Natl. Acad. Sci. USA 108, 13281–13286. https://doi.org/10.1073/pnas.1105108108.

R Core Team, 2022. R: A Language and Environment for Statistical Computing. R Foundation for Statistical Computing, Vienna, Austria. https://www.R-project.org/.

Rotaru, D.C., Lewis, D.A., Gonzalez-Burgos, G., 2012. The role of glutamatergic inputs onto parvalbumin-positive interneurons: relevance for schizophrenia. Rev. Neurosci. 23 https://doi.org/10.1515/revneuro-2011-0059.

Ruden, J.B., Dugan, L.L., Konradi, C., 2021. Parvalbumin interneuron vulnerability and brain disorders. Neuropsychopharmacology 46, 279–287. https://doi.org/10.1038/s41386-020-0778-9.

Salvatore, M., Wiersielis, K.R., Luz, S., Waxler, D.E., Bhatnagar, S., Bangasser, D.A., 2018. Sex differences in circuits activated by corticotropin releasing factor in rats. Horm. Behav. 97, 145–153. https://doi.org/10.1016/j.yhbeh.2017.10.004.

Sanchez, E.O., Bangasser, D.A., 2022. The effects of early life stress on impulsivity. Neurosci. Biobehav. Rev. 137, 104638 https://doi.org/10.1016/j.neubiorev.2022.104638.

Santiago, A.N., Lim, K.Y., Opendak, M., Sullivan, R.M., Aoki, C., 2018. Early life trauma increases threat response of peri-weaning rats, reduction of axo-somatic synapses formed by parvalbumin cells and perineuronal net in the basolateral nucleus of amygdala. J. Comp. Neurol. 526, 2647–2664. https://doi.org/10.1002/cne.24522.

Schiavone, S., Sorce, S., Dubois-Dauphin, M., Jaquet, V., Colaianna, M., Zotti, M., Cuomo, V., Trabace, L., Krause, K.-H., 2009. Involvement of NOX2 in the development of behavioral and pathologic alterations in isolated rats. Biol. Psychiatr. 66, 384–392. https://doi.org/10.1016/j.biopsych.2009.04.033.

Sohal, V.S., Zhang, F., Yizhar, O., Deisseroth, K., 2009. Parvalbumin neurons and gamma rhythms enhance cortical circuit performance. Nature 459, 698–702. https://doi.org/10.1038/nature07991.

Sorg, B.A., Berretta, S., Blacktop, J.M., Fawcett, J.W., Kitagawa, H., Kwok, J.C.F., Miquel, M., 2016. Casting a wide net: role of perineuronal nets in neural plasticity. J. Neurosci. 36, 11459–11468. https://doi.org/10.1523/JNEUROSCI.2351-16.2016.

Spijker, S., Koskinen, M.-K., Riga, D., 2020. Incubation of depression: ECM assembly and parvalbumin interneurons after stress. Neurosci. Biobehav. Rev. 118, 65–79. https://doi.org/10.1016/j.neubiorev.2020.07.015.

Stoltenborgh, M., Bakermans-Kranenburg, M.J., Alink, L.R.A., van Ijzendoorn, M.H., 2015. The prevalence of child maltreatment across the globe: review of a series of meta-analyses: prevalence of child maltreatment across the globe. Child Abuse Rev. 24, 37–50. https://doi.org/10.1002/car.2353.

Takahashi, A., 2022. The role of social isolation stress in escalated aggression in rodent models. Neurosci. Res. S0168010222002127. https://doi.org/10.1016/j.neures.2022.07.009.

Takamori, S., Rhee, J.S., Rosenmund, C., Jahn, R., 2001. Identification of differentiation-associated brain-specific phosphate transporter as a second vesicular glutamate transporter (VGLUT2). J. Neurosci. 21, RC182. https://doi.org/10.1523/JNEUROSCI.21-22-j0002.2001. RC182.

Takamori, S., Rhee, J.S., Rosenmund, C., Jahn, R., 2000. Identification of a Vesicular Glutamate Transporter that Defines a Glutamatergic Phenotype in Neurons 407.

Tóth, M., Halász, J., Mikics, É., Barsy, B., Haller, J., 2008. Early social deprivation induces disturbed social communication and violent aggression in adulthood. Behav. Neurosci. 122, 849–854. https://doi.org/10.1037/0735-7044.122.4.849.

Toth, M., Mikics, E., Tulogdi, A., Aliczki, M., Haller, J., 2011. Post-weaning social isolation induces abnormal forms of aggression in conjunction with increased glucocorticoid and autonomic stress responses. Horm. Behav. 60, 28–36. https://doi.org/10.1016/j.yhbeh.2011.02.003.

Toth, M., Tulogdi, A., Biro, L., Soros, P., Mikics, E., Haller, J., 2012. The neural background of hyper-emotional aggression induced by post-weaning social isolation. Behav. Brain Res. 233, 120–129. https://doi.org/10.1016/j.bbr.2012.04.025.

Trainor, B.C., Takahashi, E.Y., Silva, A.L., Crean, K.K., Hostetler, C., 2010. Sex differences in hormonal responses to social conflict in the monogamous California mouse. Horm. Behav. 58, 506–512. https://doi.org/10.1016/j.yhbeh.2010.04.008.

Tremblay, R., Lee, S., Rudy, B., 2016. GABAergic interneurons in the neocortex: from cellular properties to circuits. Neuron 91, 260–292. https://doi.org/10.1016/j.neuron.2016.06.033.

Troller-Renfree, S., McDermott, J.M., Nelson, C.A., Zeanah, C.H., Fox, N.A., 2015. The effects of early foster care intervention on attention biases in previously institutionalized children in Romania. Dev. Sci. 18, 713–722. https://doi.org/10.1111/desc.12261.

Ueno, H., Suemitsu, S., Murakami, S., Kitamura, N., Wani, K., Okamoto, M., Matsumoto, Y., Ishihara, T., 2017a. Region-specific impairments in parvalbumin interneurons in social isolation-reared mice. Neuroscience 359, 196–208. https://doi.org/10.1016/j.neuroscience.2017.07.016.

Ueno, H., Suemitsu, S., Okamoto, M., Matsumoto, Y., Ishihara, T., 2017b. Parvalbumin neurons and perineuronal nets in the mouse prefrontal cortex. Neuroscience 343, 115–127. https://doi.org/10.1016/j.neuroscience.2016.11.035.

van Harmelen, A.-L., van Tol, M.-J., van der Wee, N.J.A., Veltman, D.J., Aleman, A., Spinhoven, P., van Buchem, M.A., Zitman, F.G., Penninx, B.W.J.H., Elzinga, B.M., 2010. Reduced medial prefrontal cortex volume in adults reporting childhood emotional maltreatment. Biol. Psychiatr. 68, 832–838. https://doi.org/10.1016/j.biopsych.2010.06.011.

van Heukelum, S., Mogavero, F., van de Wal, M.A.E., Geers, F.E., França, A.S.C., Buitelaar, J.K., Beckmann, C.F., Glennon, J.C., Havenith, M.N., 2019. Gradient of parvalbumin- and somatostatin-expressing interneurons across cingulate cortex is

differentially linked to aggression and sociability in BALB/cJ mice. Front. Psychiatr. 10, 809. https://doi.org/10.3389/fpsyt.2019.00809.

Vereczki, V.K., Veres, J.M., Müller, K., Nagy, G.A., Rácz, B., Barsy, B., Hájos, N., 2016. Synaptic organization of perisomatic GABAergic inputs onto the principal cells of the mouse basolateral amygdala. Front. Neuroanat. 10 https://doi.org/10.3389/fnana.2016.00020.

Võikar, V., Polus, A., Vasar, E., Rauvala, H., 2004. Long-term individual housing in C57BL/6J and DBA/2 mice: assessment of behavioral consequences: effect of isolation on mouse behavior. Gene Brain Behav. 4, 240–252. https://doi.org/10.1111/j.1601-183X.2004.00106.x.

Wang, H.-X., Gao, W.-J., 2010. Development of calcium-permeable AMPA receptors and their correlation with NMDA receptors in fast-spiking interneurons of rat prefrontal cortex: Ca $^{2+}$ -permeable AMPA receptors in cortical interneurons. J. Physiol. 588, 2823–2838. https://doi.org/10.1113/jphysiol.2010.187591.

Wukitsch, T.J., Brase, E.C., Moser, T.J., Kiefer, S.W., Cain, M.E., 2020. Differential rearing alters taste reactivity to ethanol, sucrose, and quinine. Psychopharmacology 237, 583–597. https://doi.org/10.1007/s00213-019-05394-x.

Yamada, J., Ohgomori, T., Jinno, S., 2015. Perineuronal nets affect parvalbumin expression in GABAergic neurons of the mouse hippocampus. Eur. J. Neurosci. 41, 368–378. https://doi.org/10.1111/ejn.12792.

Yang, Y., Raine, A., 2009. Prefrontal structural and functional brain imaging findings in antisocial, violent, and psychopathic individuals: a meta-analysis. Psychiatry Res. Neuroimaging. 174, 81–88. https://doi.org/10.1016/j.pscychresns.2009.03.012.

Yizhar, O., Fenno, L.E., Prigge, M., Schneider, F., Davidson, T.J., O'Shea, D.J., Sohal, V. S., Goshen, I., Finkelstein, J., Paz, J.T., Stehfest, K., Fudim, R., Ramakrishnan, C., Huguenard, J.R., Hegemann, P., Deisseroth, K., 2011. Neocortical excitation/inhibition balance in information processing and social dysfunction. Nature 477, 171–178. https://doi.org/10.1038/nature10360.